Ultrafast Optics Study of Coherent Acoustic Phonons and Carriers in High Quality Silicon on Glass Sample

By

Magaña Loaiza Omar Santiago

A Dissertation Submitted to the program in Optics, "Optics Department"

in partial fulfillment of the requirements for degree of

Master of Science in Optics

at the

National Institute for Astrophysics, Optics and Electronics

July_2010

Tonantzintla, Puebla

Supervised by:

Prof. José Javier Sánchez Mondragón[1],
Prof. Roman Sobolewski[2],

[1]Optics Department INAOE

[2]Department of Physics
University of Rochester

Index content

Figures Index

Agradecimientos

Mi más fuerte agradecimiento y respetos a quien ha sido mi maestro, tutor y amigo; el Dr. Javier Sánchez Mondragón, a quien admiro mucho y quien afortunadamente me ha orientado y apoyado como un padre por el camino de la vida y la ciencia; me ha dedicado su valioso tiempo y regalado sus apreciables y únicas lecciones de vida, que para mi resultan extraordinarias y que he tratado de poner en práctica cada día de mi existencia.

También comentar que aprecio las oportunidades que CONACyT ofrece para la comunidad estudiantil; agradezco el apoyo brindado a través de la beca otorgada para realizar mis estudios de maestría y el programa de becas mixtas para estudiantes en el extranjero; además a quienes tuve la oportunidad de contactar personalmente expreso un afectuoso agradecimiento al Lic. Jorge Ochoa de becas Internacionales por haberme brindado el mejor servicio y haberme guiado para solicitar el apoyo requerido; al igual que a la Lic. Gabriela Gómez Gutiérrez de Becas Mixtas Nacionales por su apoyo; por último agradezco en particular al Dr. Luis Gil Cisneros a quien no tuve la oportunidad de corresponder personalmente, sin embargo le agradezco haberme guiado y mostrado tanto interés en mi desarrollo.

Agradezco también al Prof. Roman Sobolewski y su grupo de estudiantes, que me brindaron la oportunidad de realizar una estancia de investigación en la Universidad de Rochester, N.Y. misma estancia que me permitió sentar las bases para elaboración de esta tesis, que en conjunto con la gran dedicación que me ha demandado, me ha brindado la oportunidad de realizar un Doctorado en Artes y Ciencias y una distinguida beca de la misma Institución que me permitirá continuar realizando mis estudios.

Es importante agregar que parte de mi gratificación hacia el profesor Sobolewski es debido al apoyo y consejos que me concedió y fueron claves para mi éxito obtenido en la Universidad de Rochester; además agradezco a mi amigo y compañero de piso Adam Sobolewski y su mamá Bozena de los que además recibí un gran apoyo.

Quisiera mencionar mi agradecimiento al Prof. Joseph Eberly por sus valiosos consejos, que me permitieron ver la ciencia desde una perspectiva única, y tomar decisiones importantes relacionadas con mi carrera científica.

Así mismo me siento afortunado de haber sido recibido y entrenado en la parte de laboratorio por los estudiantes de doctorado Jie Zhang y Hiroshi Irie por su gran apoyo en el laboratorio y sus consejos de estudiante a estudiante, cabe mencionar que estoy sumamente impresionado por la mente y el talento de Hiroshi Irie, del cual aprendí mucho mientras convivíamos juntos.

En el fondo de mi corazón agradezco a mis padres Santiago Magaña Vázquez y Carmen Loaiza Reynaldo a quien tanto admiro, y son un modelo a seguir tanto como padres como amigos, y yo realmente no tengo como agradecerles por todo lo que han hecho por mí siempre, cabe mencionar que siempre he tenido de su parte un apoyo incondicional en todos los sentidos y en cada momento de las duras lecciones de mi vida.

Otras personas muy importantes para mí y que deseo agradecer son mi hermano Carlos Magaña Loaiza, mi querida novia Paloma Ybarra Reyes y a mi abuelita Kika Reynaldo, por su paciencia y que siempre han estado preocupados y a la expectativa de ver en qué modo pueden apoyarme, y de los cuales he recibido consejos y grandes ayudas.

Para finalizar, agradezco a Dios y a la Virgen de Guadalupe por cuidar a todos mis seres queridos, y por brindarme tantas oportunidades a lo largo de mi corta y dulce vida.

A todos ustedes mil gracias

Omar Santiago Magaña Loaiza

Acknowledgements

My deepest gratitude and respects to who has been my teacher, advisor and friend, Dr. Javier Sanchez Mondragon; whom I greatly admire and who fortunately has guided and supported me as a father in the ways of life and science. He has devoted me his valuable time and given their significant and unique lessons of life, which for me was extraordinary and I have tried to put into practice every day of my existence.

I also want to comment that I appreciate the opportunities offered by CONACyT to the students community. I appreciate the support provided through the scholarship for my graduate studies and the extraordinary opportunity in CONACyT International Interships Program, which has let to my further development at the University of Rochester. In addition to those who I had the opportunity to contact personally, I would like to express my warmest gratitude to Mr. Jorge Ochoa from the CONACyT International Fellowship department, for giving me the best help and led me to seek the required support, as well as to Ms. Gabriela Gómez Gutiérrez from the International Interships Program for her always helpful assistance, and finally I would like to express acknowledgments to others whose efforts benefited my studies. In particular to Dr. Luis Gil Cisneros whom I did not have the opportunity to met personally, but I thank him for having guided me and shown much interest in my development.

I also thank Prof. Roman Sobolewski and his group of students who gave me the opportunity to spend an internship at the University of Rochester, N.Y., same internship that allowed me to lay the groundwork to prepare this thesis, which together with the great dedication that has granted me, has given me the opportunity to make a PhD in Arts and Sciences at the UofR and receive a distinguished scholarship from the same institution that will allow me to continue with my studies. It is important to add that part of my gratitude to Professor Sobolewski is due to the support and advice he gave me and were key to my success at the University of Rochester. I also thank his family, and especially my friend and roommate Adam Sobolewski and his mother Bozena, for their warm friendship received great support.

I would like to mention my gratitude and respect to Prof. Joseph Eberly for his valuable advices, which enabled me to perceive science from a unique perspective, and to make important decisions on my scientific career.

Furthermore I feel fortunate to have been welcomed and trained in the laboratory by the graduate students Jie Zhang and Hiroshi Irie, for their great support in the lab and peer advice. I was impressed by the insight and talent of Hiroshi, from wich I learned a lot while we share lab hours together.

Deep in my heart I thank my parents Santiago Magaña Vázquez and Carmen Loaiza Reynaldo whom I greatly admire. They are role models both as parents and friends and I really don't have a way to thank them for all that they have done for me every day in my life. They have been with their unconditional support, every way and every moment, at the hard life lessons of my life.

Other very important people to me, which I want to thank for loving me and being always there are my brother Carlos Magaña Loaiza, my beloved girlfriend Paloma Ybarra Reyes and last but not the least my great love, my grandma Kika Reynaldo, thanks all for your patience and for being always worried and expectant of how can you support me, and from whom I have received great advice and love.

I thank God and to our Lady of Guadalupe for taking care of all my beloved ones, and for giving me so many opportunities throughout my sweet and short life.

A thousand thanks to all of you

Omar Magaña Santiago Loaiza

Abstract

In this thesis we characterize the carriers and phonons dynamics of a novel Silicon on Glass sample designed and constructed by Corning Inc. with the aim to be used it for photonics and electronics devices.

The dynamics of our interest occurs in a very short period of time, in the order of picoseconds and femptoseconds, which becomes the electronics instrumentation obsolete to measure such very fast signals. Therein the reason to use alternative tools such as ultrafast lasers, in real ultrafast optics.

Ultrafast optics has allowed developing important ultrafast spectroscopy techniques; in this case we use pump-probe spectroscopy, which allows studying ultrafast phenomena such as carrier and phonons dynamics.

Pump-probe spectroscopy is a nondestructive technique which consists on exciting a material with the pump beam, in our particular case, such excitation generates hot carriers, which generates changes in reflectance that are detected by the probe beams as time evolves. Such changes are due to different steps in the process to achieve an equilibrium state; every process step is particular of each material, which produces particular reflectance behavior that allows characterizing the dynamics of such material.

In this thesis we provide a theoretical model for carrier dynamics that allows the realization of other important processes such as changes in refraction index, concentration of generated carriers, and relaxation and recombination time constants.

The final part of this research consist on the generation and detection of coherent acoustic phonons by the use of pump probe experimental setups, in a similar manner to the one described above, where a pump beam was focused on the aluminum transducer film that we added on the silicon side. We demonstrated that the Al film improves the phonons generation and provides the coherent characteristic to the generated phonons.

It is important to notice that we have found quite unusual and interesting phonons. Furthermore, we propose a physical model which allows us to conclude that the created phonon spectrum is finite as a consequence of the temperature conditions when the experiment was done.

Chapter 1

Introduction

1.1 Abstract

The explanation of mesoscopic phenomena in certain material provides the opportunity to predict macroscopic behaviors of materials. In fact those formulations provide the opportunity to design and develop devices, such as electronic and photonic devices.

Therein the importance of study mesoscopic phenomena such as carriers and phonons dynamics, those parameters allows predicting certain key properties of the material under study. Then one can judge the possibility to develop devices with such material.

The development of new materials such as silicon on glass brings the possibility to create novel technologies; here the necessity to understand carrier and phonon dynamics in this high quality silicon on glass material.

Due to the nature of the research done in this thesis, the first part of this chapter is used to briefly describe the importance and behavior of carriers in silicon and their impact in device performance. Then the second section briefly reviews the nature of phonons, which is going to be studied in detail in chapter 4. Finally the fabrication and structure of the studied sample is provided.

1.2 Carrier Dynamics in Semiconductors

Since the 20th century, when semiconductors technologies were discovered, science and technology has suffered incredible changes. That brought the creation of new technologies, as well as the development of new tools to study important issues that fueled the continuous advancement of this important field, and again new semiconductors technologies.

Research on carrier dynamics provides information on the behavior and interaction of the carriers with the material under study, on the design on new materials and therein new devices. They provoked collective phenomena, resulting in interesting properties that define important characteristics of those devices. The obtained information can be related with scattering processes and with the carriers' energy loss, due to deformation potential interactions resulting on the emission of phonons, which strongly influence the electron mobility [1]. The fundamental parameters that define the semiconductor devices operation, such as the saturation velocity that determine how fast they will operate and are closely related with the electron mobility and the phonons dynamics.

If we are interested on the formulation of the carriers motion on a single crystal, we need a good crystal description as the one provided by the Kroning-Penney model. There, the crystal lattice is conceived as a periodic potential function, whose Schrodinger equation can be solved with the aid of the Bloch theorem. Therefore carriers or in this case electrons, just can occupy discrete allowed energy levels or bands. In particular, in silicon we find them in a k-space described by the following diagram, see Fig 1.

It is easy to realize, that for silicon the maximum value of energy for valence band and minimum conduction band energy value does not

correspond to same k-value. This situation is known as indirect band gap, and this fact brings as a consequence a different carrier dynamics.

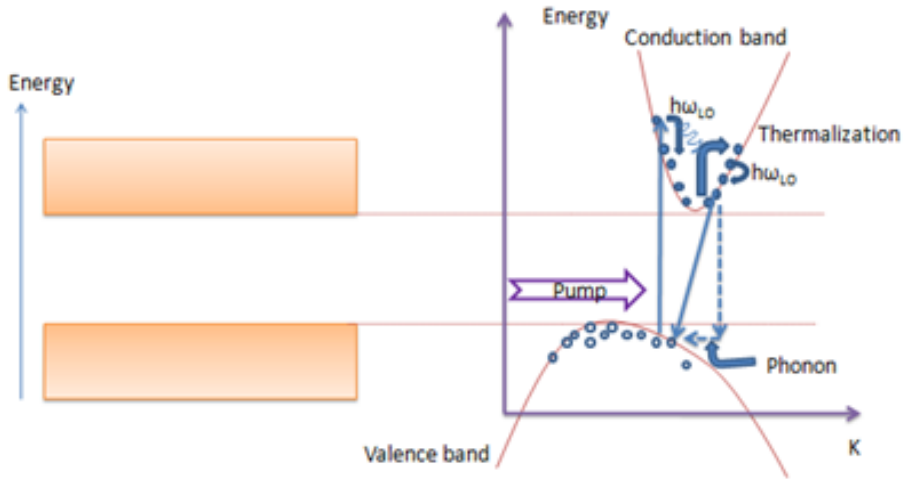

Fig 1. Representation of silicon band diagram structures, in k space diagram are sketched the different stages generated after an excitation pulse.

Using basic postulates from quantum statistics [2], we know that identical indistinguishable particles of half odd integral spin, like electrons and holes, are known as fermions. They satisfy the Pauli Exclusion Principle and cannot occupy the same quantum states and their occupancy probability in each band can be described by Fermi-Dirac statistics.

From figure 1, one can notice that after exciting hot carriers, it starts a process to achieve an equilibrium state, and this process can be understood on four fast stages. The first two stages are very fast, of the order of just some picoseconds. They consist in a relaxation process, then accompanied by cooling and a loss of energy by optical phonons.

Before continuing is important to stress the conservation of energy and momentum, this law is quite evident in indirect band gap semiconductors

where exchange of momentum cannot be accompanied by emission of photons, but this is accompanied by emission of longitudinal acoustic phonons with a large momentum but small energies. For that reason, silicon has a lower radiative recombination.

The third stage consists in generation of acoustics phonons, in order to cool the lattice, and finally the longer and last stage is the recombination process which takes around 110 ps in Silicon on Glass. This is, because carriers have to travel through the bandgap in order to recombine with their counterpart.

1.3 Coherent Acoustic Phonons in Semiconductors

In a natural way, atoms in a crystal tend to oscillate when temperature changes, producing a wide spectrum of these vibrations. An elementary quantum of the atomic vibrational energy in the crystal is called a phonon [3].

When a heat pulse is applied to crystalline material interesting phenomena can be produced, in fact this interaction can be studied from different angles, just because a crystal can be considered as a macroscopic quantum system this fact allows to analyze and see interesting natures and consequences of this interaction. One of these consequences is the generation of phonons, which depending of the dominant phenomena this can be described from quantum or classical formalism.

In this thesis, we use a femptosecond laser pulse to generate them. At very low temperatures this pulse is a ballistic pulse, but at room temperature it can generate a wide spectrum of phonons. As it will be explained in Chapter 4, there are different kind of phonons; acoustic and optical phonons with different transversal and longitudinal modes.

Phonons propagation or oscillations of the atoms in the lattice produces changes in stress and strain properties therein changes in the reflectivity properties, the object to be measured in our experiment.

As we have stated, heat pulses and their thermal expansion play a key role in the generation of phonons. On the other hand, is known that laser pulse is not well absorbed in silicon, and it is not possible to generate a strain pulse composed by longitudinal acoustic phonons, but we can achieve such pulse using a material that provides good thermal expansion, this material is called a transducer.

In this research a 30 nm aluminum transducer was added to the silicon face of the silicon on glass sample, this is in order to improve the phonon generation.

One important parameter is related with the characteristic impedance of the materials, in this case between aluminum and silicon, the impedance difference plays an important role in the reflection and transmission coefficients [4].

1.4 Brief review of research on Silicon on Insulator and Silicon on Glass

We live in an age where silicon technology has played a critical role. In spite of all the enhancements that seem to situate this technology on the verge, it is quite impressive the range of new trends which allow us to overcome those frontiers and the traditional perception that silicon technologies is restricted to the electronic industry. In these days we can conceive a fruitful photonics technology and its fusion with electronic technology, furthermore the useful compatibility between those intrinsic

developments of either one of them. This could be the case of compatibility between integrated circuits (IC) technology and integrated optics based on silicon on insulator (SOI) wafers [5].

It is important to point out that the SOI technology, consisting on a film of a single crystalline Si separated by a layer of SiO2 from the bulk substrate, has been improved during the past 3 decades. For that reason, scientist have developed an impressive number of methods like Smart cut [6] and separation by implanted oxygen (SIMOX) [7]. But, out of those, the one that has reached an industrial level is SIMOX [8], therein its importance.

During all the time spent on those improvements, scientists have found important dielectrics like zirconia, calcium fluoride, spinel, sapphire, etc. The oldest is the silicon on sapphire [7], despite the numerous improvements; its quality was always inferior to bulk silicon. As a consequence, it brought many other failed efforts that culminated on high quality silicon on glass wafers.

Part of the good reasons to use silicon is that this element offers many interesting properties such as:

- a high thermal conductivity (~10× higher than GaAs),
- a high optical damage threshold (~10× higher than GaAs), and
- a high third-order optical nonlinearities. Kerr effect is 100 times larger, whereas Raman Effect is 1000 times stronger than those in silica [5].

Nowadays many optical and electronic devices have demonstrated to be ubiquitous, and fortunately silicon on glass has been improving the performance of devices like ICs and Photonic Integrated Circuits (PICs). This fact has brought the possibility to increase the integration capability, reduce undesired capacitance, radiation hardness, and same consumptions requirements as well as an increase lifetime of the devices.

In order to make studies about carrier dynamics and longitudinal acoustic phonons, which are the main aim of this thesis, I received high quality silicon on glass samples from Dr. Carlo Kosik Williams; a Corning Incorpotated. researcher [9] and a Prof Sobolewski group member.

The studied samples allows fabricating improved thin-film silicon transistors as well as displays devices [10], this is possible due to a unique method of fabrication designed by Corning Incorpotated.

This special issue is given by an unusual barrier layer which cannot be synthesized by other glass forming process mechanism [9], which prevents the diffusion of mobile ions and as a consequence promises to improve thin-film transistors as well as displays with high performance.

Fabrication of SiOG substrates starts with Corning EAGLE XG™ display glass sheets and single-crystalline silicon wafers as raw materials. The silicon is first implanted with hydrogen ions to a desired depth, defining an atomic separation plane in the wafer. Both the glass and silicon wafers are then cleaned and pre-bonded via Van der Waals force. The pre-bonded silicon/glass system is subsequently subjected to heat and voltage in an anodic bonding process that causes a separation of the silicon layer at the hydrogen implant plane, and further results in an extremely strong and stable bond between the transferred silicon film and underlying glass, see Fig 2.

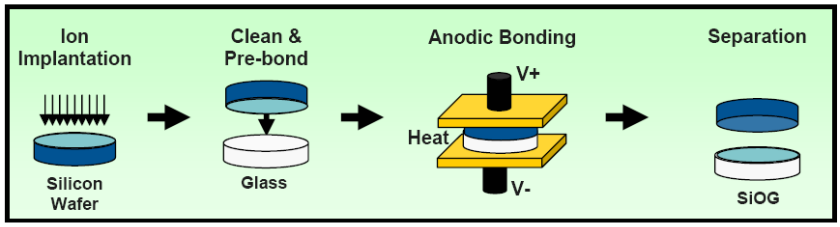

Fig 2. Corning® Silicon-on-Glass (SiOG). Fabrication process taken from [11]

During the anodic bonding process, the heating also increases the mobility of the ionic constituents in the glass and the electric field induces drift of these ions. Oxygen ions move toward and react with the silicon to form a thin SiO2 layer which enhances the adhesion between the silicon and glass. At the same time, glass network modifiers such as Mg+, Sr+, Ca+ move away from the silicon to form a mobile ion free zone and a buried ion accumulation zone in the glass substrate. This unique combination of Si/SiO2/ion-free zone is critical for functional TFTs because it provides a barrier layer that prevents ion migration from the glass that would otherwise contaminate devices fabricated in the silicon. As a result, SiOG can be described as a five-layer structure: (1) the transferred single crystal silicon thin film, (2) an electrochemically formed SiO2 layer of ~10 nm, (3) a mobile ion free zone of ~100 nm, (4) an ion accumulation zone, and (5) the base glass.

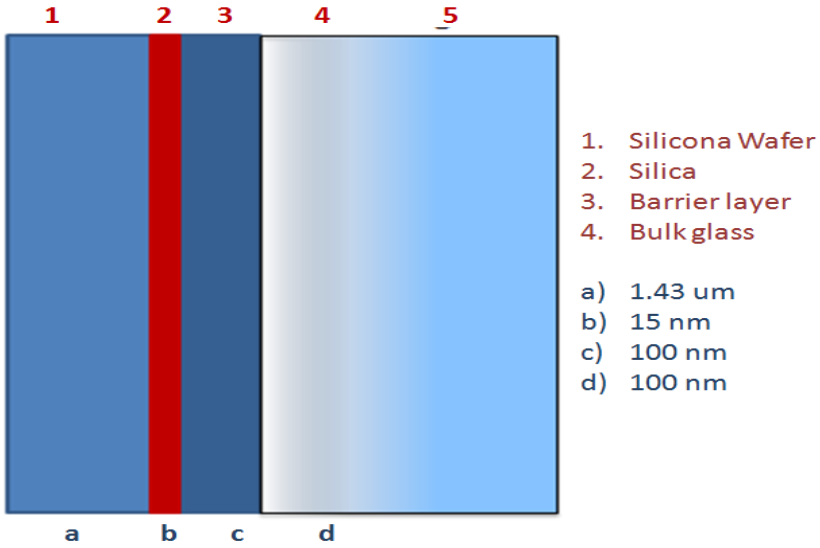

Fig 3 Silicon on Glass simple structure

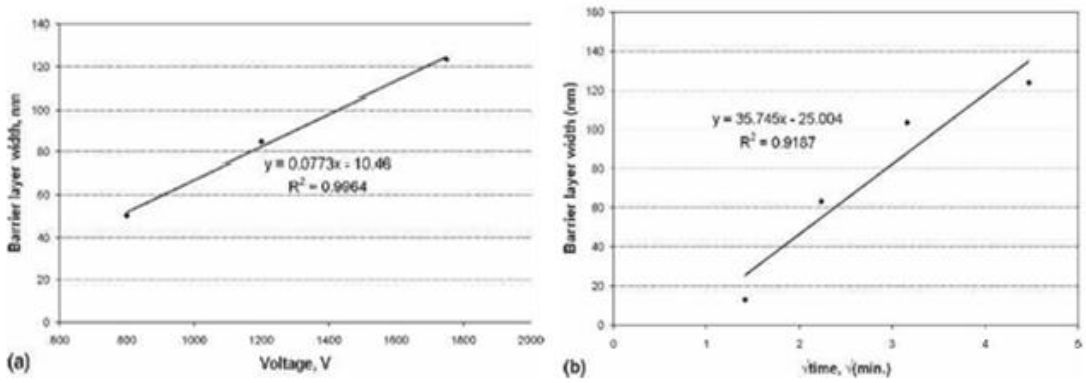

Fig 4. a) Dependence of barrier layer with applied voltage. b) Dependence of barrier layer with square root of time. Taken from Kosik Williams, C. paper [11].

Finally is important to stress that barrier layer growth is a function of applied voltage at 575^{o} C / 20-min process cycle, and as a function of time at 575 ^{o} C/1750 V. This is shown in Fig. 4.

Chapter 2

Experimental Setup

2.1 Abstract

The interests on describing carrier dynamics and studies on phonons requires of an experimental setup and instruments with the ability to pursue such phenomena and the capability to measure it. That experimentally means to be well within those scales of time. Typical phonon dynamics are well within picoseconds, therefore we need pulsed lasers much shorter than this to excite them and detections systems well into the range.

Unfortunately electronic instrumentation is not fast enough to detect such reactions but light signals are fast enough to measure them and become a handy tool toward that aim. There, the work developed by many scientists in ultrafast characterization, such as the pump probe technique, allows studying such phenomena.

The Pump probe technique is an interesting technique which allows nondestructively testing materials by detecting changes in the reflectance or the transmittance with a high temporal resolution (picoseconds), which are strongly related with energy transport phenomena in a given material, such as semiconductors or metals. Therefore, we belive that an explanation on the fundamental elements used in this technique and to stress the importance of those elements and the physics behind them is required, in order to have a

full understanding of why pump probe experiments can help to study our phenomena.

We are going to give a thorough description of the short pulse light source and the detection technique to be used on the different schemes of the experimental setup of the pump probe technique.

2.2 Lasers System

The most important objective, in this thesis, it is to describe carrier dynamics and to generate and detect longitudinal acoustic phonons. Those processes occur in a very short range of time that goes from some picoseconds to hundred picoseconds.

Therefore the pulses should have a shorter duration than the entire process. To produce such instrument is not an easy task, and definitely not available at our institute yet, therefore and for the sake of my fellow students I will briefly describe the amplifying materials and the techniques used to compress the pulse.

The previous situation is satisfied using a femptosecond mode locked laser, in this case we used a Coherent MiraTM 900 ultrafast laser which is a femptosecond mode locked Ti:Sapphire solid state laser with a wide wavelength tunable range in the near infrared, long term stability and the capability to provide ultra-short pulses of 100 fs. This particular laser offers interesting features that allows using them in time domain spectroscopy studies.

To support a short pulse generation the amplifying material has to be spectrally broad, therefore it is quite natural to consider semiconductor

materials. Nowadays spectroscopic studies on semiconductor materials are very important and interesting properties such as the material response with the excitation energy are important research lines.

The energy level reached by the light used to excite the material, taking as a reference the energy band gap and its relative position in the bands structure, allows us to study different semiconductor behaviors.

In that circunstance the convenience of having a tunable laser, such as the laser used on the development of this thesis, since it provides great freedom for spectroscopy research. Solid state laser is a classification used to refer to all the lasers whose gain medium is typically formed by metal ions and a dielectric host material [12] such as Ti+3:Al2O3, in fact this is the most commonly used solid state tunable laser. In order to obtain Ti+3:Al2O3 a chemical reaction between Ti2O3 and Al2O3 is required. This produces the substitution of Ti3+ in Al ions in the lattice.

The Ti electronic configuration can be written as 1s2 2s2p6 3s2p6d2 4s2, when titanium becomes Ti3+ it transfers the last 3 electrons in order to form an ionic bonding with octahedral geometry [13]. The fivefold degenerate d-electron levels are split by the crystal field of the oxygen anions (ions with negative density of charge), into a triply degenerate 2T2 ground state and a doubly degenerate 2E excited state. One important point to discuss is related with the absorption and emission range, in Ti: Sapphire laser those parameters are determined by the energy states distance, such states determine absorption and fluorescence bands [14], see fig 5.

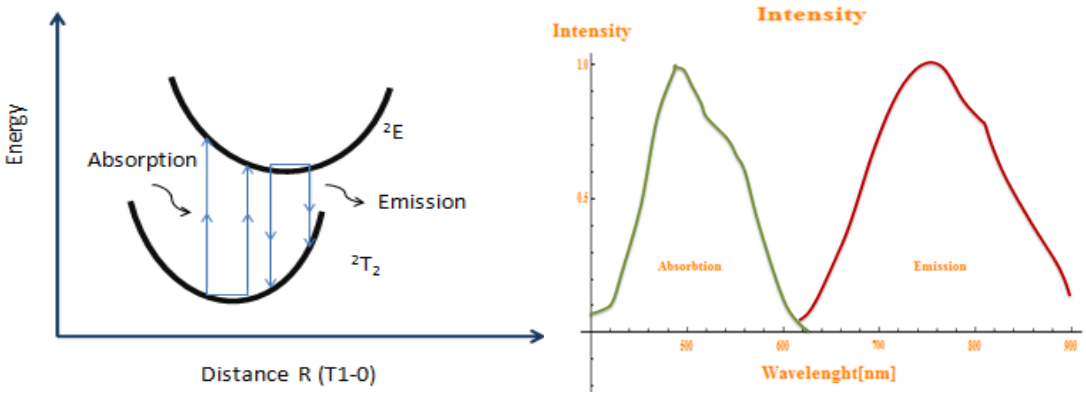

Fig.5A. Energy band diagram of TI^{+3} in Sapphire. 5B. Absorption and emission spectrum of Ti $^{+3}$In Sapphire.

The absorption spectra range covers an interval from 400 nm to 650 nm and the fluorescence range goes from 600 nm to 1050 nm as it is illustrated in figure 5. Therein this overlap between absorption and emission is only possible to lasing from 700 nm to 1050 [15].

From figure 5B is easy to see that we have strong absorption near to 500 nm, which means that in order to produce population inversion is convenient to pump near to 500 nm. Therein the need to add one more key element in our laser system; this element is a VERDITM V-10 green laser, which is used to pump the Coherent MiraTM 900 [16], see Fig 6. VERDITM V-10 is a frequency-doubled diode-pumped solid-state Continuous wave (CW) green laser which provides a wavelength of 532 nm with a power up to 10 W.

When a laser system is described, a good part of it is related with fundamental physics (atomic systems, quantum states or modes, population inversion, solid state physics of the active medium, etc) but the laser needs of engineering, like the one used to achieve mode locking configuration with pulses during around 100 femptoseconds using Kerr lens mode locking (KLM) [17].

The actual building up of a short pulse, as short as a hundred femtoseconds requires different mechanism such as mode locking. Therefore, before continuing it is important to describe how mode locking configuration is achieved and configured to do the desired spectroscopy.

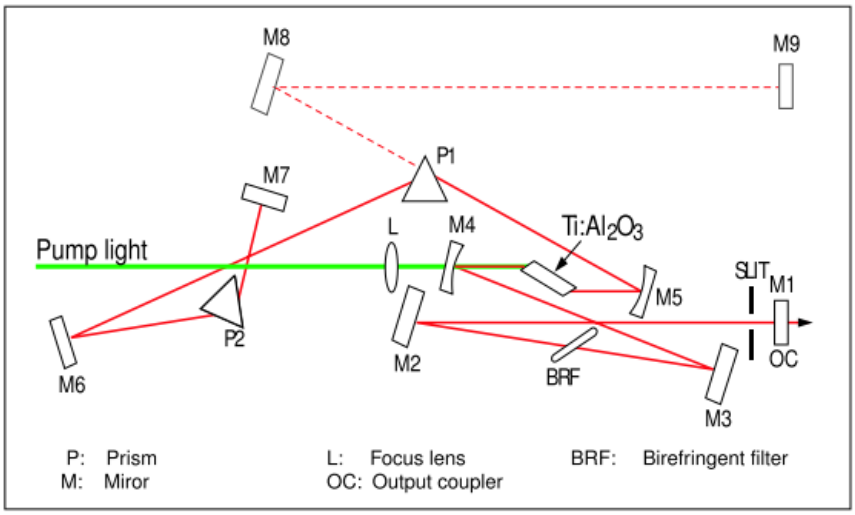

Fig.6. Optical design diagram of Coherent MiraTM 900, figure taken from the Coherent Mira Manual

As can be observe from figure 6, mirrors M7 and M1/OC form the Mira laser cavity. If the laser is operating in a mode locking configuration that means that inside the cavity exists many optical modes, and those modes are generated by CW pump laser, which is the green line in Fig 6.

In order to start building up a model for this configuration, we can start by considering the different modes inside the cavity, and then each mode will have a phase which under normal circumstances is randomly changing.

In spite of the randomness of the modes in the cavity, an interesting situation is achieved. In order to understand how that situation can be obtained; we can start with the mathematical form of the laser outside the cavity as follows: [18].

$$E(t) = \sum_{m=-n}^{+n} E_0 \, e^{\{i[(\omega_0 + m\Delta\omega)t + \varphi_m]\}}. \quad (1)$$

Here ω_0 is the central mode frequency and the remaining terms are part of the phase which is different for each mode, in fact this part stress the randomness of the phase, which can be divided into two components $\Delta\omega$ and φ_m defined as the frequency difference of two consecutive modes and the phase of the central modes respectively.

In order to achieved an expression which allows figuring out the physics of certain phenomena we can include the phase and the amplitude E_0 in generalized amplitude$A(t)$, rewriting the expression 1 as follow:

$$E(t) = A(t)e^{\{i\omega_0 t\}} \quad \text{Where} \quad A(t) = \sum_{m=-n}^{+n} E_0 \, e^{\{i[m\Delta\omega t + \varphi_m]\}}. \quad (2)$$

It is easy to recognize that we can parametrize the time dependent amplitude by changing the argument by $\Delta\omega t'$ and then using the convergence of the recognized geometric progression by the morphology of the amplitude. We can rewrite the amplitude as follow [19]:

$$A(t') = E_0 \frac{Sin[(2n+1)\Delta\omega t'/2]}{Sin(\Delta\omega t'/2)}. \quad (3)$$

Finally the intensity can be written as:

$$I = E(t) * E^*(t) = |E_0|^2 \frac{Sin^2[(2n+1)\Delta\omega t'/2]}{Sin^2(\Delta\omega t'/2)}. \quad (4)$$

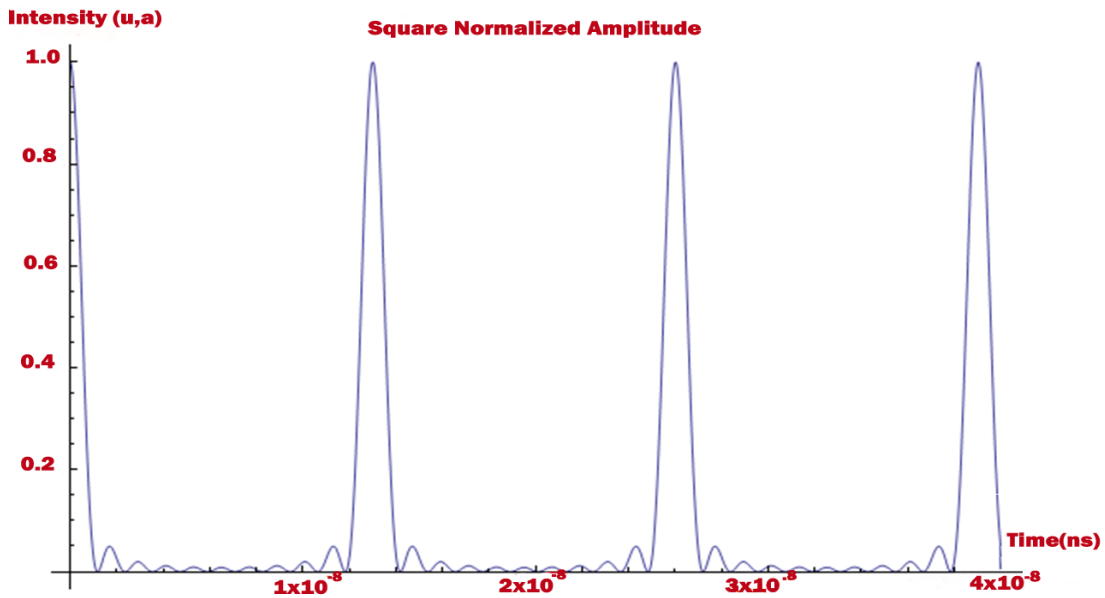

Fig 7.A. Plot of the normalized intensity with locked phases and equal amplitude. Using 10 oscillating modes

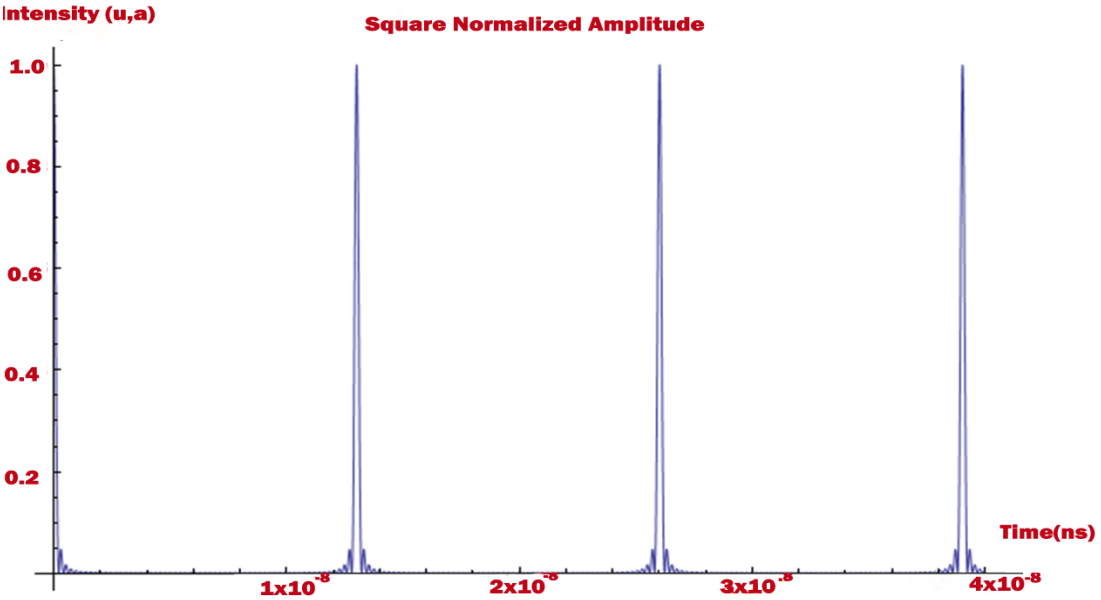

Fig 7.B Plot of the normalized intensity with locked phases and equal amplitude. Using 25 oscillating modes.

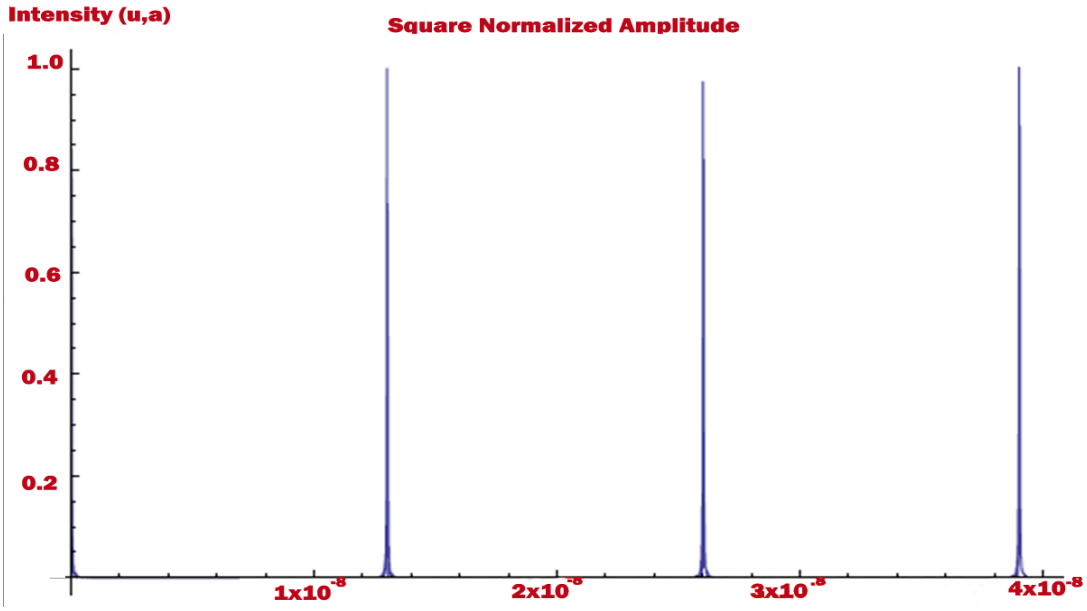

Fig.7C. Plot of the normalized intensity with locked phases and equal amplitude. Using 50 oscillating modes.

After plotting the intensity, is clear the influence of the number of oscillating modes. In fact they have a constant phase differences, then the possibility to have the interference as shown in Fig 7.

For this kind of cavity there exists a condition over the wave number. Stationary solutions exist only when k satisfies the boundary conditions. This condition is perfectly natural and can be achieved taking into account $k = \omega/c$, then introducing this relation and treating the cavity problem as an eigenvalue problem, it can be obtained that (λ/2)n=L which says that a stationary condition can be achieved only for those vibrations that contains an integer number of half wavelength along the string, otherwise the destructive interference between direct and reflected wavelength in the cavity mirrors cancel them [20]. It is important to mention that wavelengths which satisfy such condition have constructive interference.

Then one can conclude that the vibration frequencies (or vibration spectrum) are the harmonics given by $\omega_n = \frac{2\pi c}{\lambda_n} = (c\pi/L)n$ and fundamental frequency of vibration is given by $v_1 = c/2L$ or $\tau_1 = 2L/c$. That in a Mira 900 corresponds to 13.2 ns which gives a repetition rate of 76MHz.

It is quite attractive the application of nonlinear optics, in fact the entire optical system that have been used to develop this research make uses of two interesting properties; those are the Kerr nonlinearity and the second harmonic generation. The first is going to be discussed in order to complete the description of laser Mode locking configuration, and the second is going to be described later.

Kerr lens mode locking uses the principle of Kerr effect, which is the characteristic nonlinear susceptibility response [21] of a given material to electromagnetic fields applied on such material. This response shows as changes in the refractive index as a function of the intensity used to illuminate the material. This phenomena has the following mathematical form$n = n_0 + n_I I$. Where n_0 is the linear part, which is independent of intensity, n_I is the nonlinear response and I is the intensity of the light.

Under the assumptions made by T. Brabec et al [22], it is clear that a nonlinear index of refraction produces intensity-dependent focusing but also inhibits dispersion. Considering a phase temporally varying pulse, with an average velocity equal to group velocity, it is known that it will experiment different velocities, producing the opposite effect to a group velocity dispersion. This is because depending on the time dependent intensity the pulse travels with different velocities where the edge with small intensity travels faster than the part with high intensity, acting as a pass band filter and making the pulse narrower.

Here it is important to stress that depending of the engineering used, the mode locking technique is classified in passive and active techniques. In the first the mode locking element is formed inside the cavity using a nonlinear effect. In the second an external element is used to achieve the mode locking configuration.

The Mira 900 Laser uses a passive mode locking, using the active medium as a KLM. Ti:Sapphire forms a self Kerr lens effect which improves the performance of the cavity.

Analyzing the cavity and the KLM as a problem of harmonics, which can be reflected in a non constant phase which varies with the time, one can start to take into account problems generated as a consequence of the difference between group velocity and phase velocity. In fact here the group velocity changes with the time due to different velocities superposed to form the group.

Actually this fact brings the possibility to have significant positive group velocity dispersion (GVD) [23]. That is the reason to have two Brewster prisms in order to compensate the positive GVD. Those prisms allow tuning the laser pulse width.

2.3 Detection System.

As we mentioned before, the main aim of this work is to investigate carrier and phonons dynamics that is an ultrafast phenomena. Then our tools to study them should also be very fast in order to have an accurate picture of a given phenomenon. In fact the electronics equipment available to measure fast phenomena is not fast enough to be used in the research done in this thesis. This problem is due to the bandwidth limitation of the electronic circuits

(high bandwidth means short pulses, the bandwidth becomes wider as the pulses become shorter). In fact it is impossible to measure the transients of interest with conventional real time oscilloscopes.

2.4 Optical Sampling System

It is well known that the frequencies used in electronic and electrical circuits field are very small in comparison with the frequencies of light. In fact this is the reason why optics is taking advantages over electronics in the communications field [24] and one of the clever issues in pump probe experiments. In order to point out the problem that we have, let us consider the picture in figure 8:

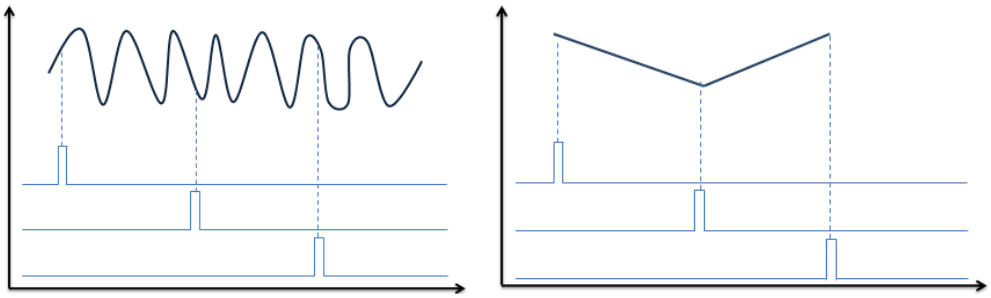

A. B.

Fig.8A. Schematics of sampling in time domain. B. Schematic of the obtained plot after sampling, which shows the inefficiency of the method in fast signals.

Figure 8-A) shows the signal of interest, which is the signal to be measured. The signal below it, formed by a series of square pulses, is used to sample the captured signal. In this case, the system could be an oscilloscope trying to capture an optical signal frequency.

The oscilloscope, as most of the electronics devices, needs a trigger signal which is a periodic signal that acts as clock pulses in order to synchronize certain device [25]. In figure (8-B) is clear that the sampling rate of the

oscilloscope is not good enough compared with the harmonic oscillations, which is the signal of interest, then the measured signal is completely different to the real signal.

In fact this situation shows how ineffective can be to sample a very fast signal with an oscilloscope, the problem is that the sample rate is slower than the signal which is going to be measured; this fact is due to limitation of bandwidth.

This means that in order to have faithful measurement a shorter pulse is needed. These pulses allow mapping with a higher repetition rate and an improved and trustily reconstructed signal.

It is well known that people have used electronic equipment to measure electronic signals, so it could be reasonable to use an optical system to measure a phenomena which is as fast as optical velocities. We previously highlighted the frequencies that can be achieved with mode locking configuration. For that the possibility to design an optical experiment with a configuration that provides the possibility of sampling fast signals in real time. In other words, to increase the bandwidth using ultra fast short pulses.

2.5 Small Signal Detection

In the following section is introduced an explanation of the entire experiment. Nevertheless a description of the key elements and the fundamental performances has been discussed in order to understand better the general performance of the entire experiment. Furthermore in the following section the remaining instruments or equipments are explained.

This section is used to explain an important part of the experiment, which deals with the signals processing. The need to apply certain operations on the signal come as a necessity to distinguish the studied signal from the noise and from other operations applied during the experiment.

One of the most common problems generated when a small optical signal used is related with the detection part and during the distinction stage. This is due to the nature of such signal and the possible sources of noise in the laboratory. In fact these sources of noise are consequences of the laser instability, scattered light in the experiment going through the detector (in fact in our experiment that was a big issue to solve), noise from the electronic devices, etc.

Before describing the signal processing, it is necessary to understand certain concepts and the operation of certain devices used to process the optical signal such as: the modulation of signals, the operation of acousto-optic modulators (AOM) and the phase sensitive detection used by a Mode lock-in amplifier.

The modulation of a signal is done in order to increase the signal to noise ratio (SNR, avoid attenuation). Basically this process consists of modifying the amplitude of a high frequency signal with, named carrier, with a low frequency signal, named modulating, which is the signal that contains the information that will be transmitted. This brings as a consequence long pulses, in fact this work is done by an acousto-optics modulator.

The AOM is an amplitude modulator which needs an electrical signal in order to modify intensity and frequency of an optical beam. The electrical signal generates sound or acoustic waves by the use of a piezoelectric transducer that interacts with the light waves. This interaction is a

consequence of refractive index changes in the optical medium by acoustic waves; those changes produce the effect of a moving sinusoidal grating. Then the light beam will be diffracted by the grating into several diffraction orders [26]. The intensity of the diffracted light is proportional to the power of the acoustic wave, and as a consequence the intensity can also be modulated.

The heart of a Lock in amplifier is a phase sensitive detection (PSD) module, as will be explained in the Pump-Probe technique section. The reason to use such device is the need to recover the signal of interest after being modulated and to discern it from the noise. PSD provides an elegant and clever way to have the opportunity to modulate and reduce noise, with the option to have changes in the frequency of excitation or modifying the bandwidth of a given filter. The phase sensitive detector can be understood in two blocks, one block of synchronization and another one of amplification and filtering.

Qualitatively speaking the first works comparing an input signal with a synchronization signal. Then the resulting signal goes to the amplification and filtering blocks and an average of the signal is computed, depending on the phase difference. Depending on the signal, as a function of the difference of phases or synchronization, is obtained a dc voltage level. In the case of a randomly changing phase, this average goes to zero.

The elements already described before interact with each other as it is shown in figure 9. A signal with a frequency of 98 KHz and amplitude of 1.3 V is used to feed the AOM and at the same time to trigger the Lock in Amplifier. After the AOM modulate the light signal, it goes through the optical system. The Lock in amplifiers then compares the triggered signal and the signal after

the optical system block by PSD, and finally sends the signal to a PC with a good SNR value.

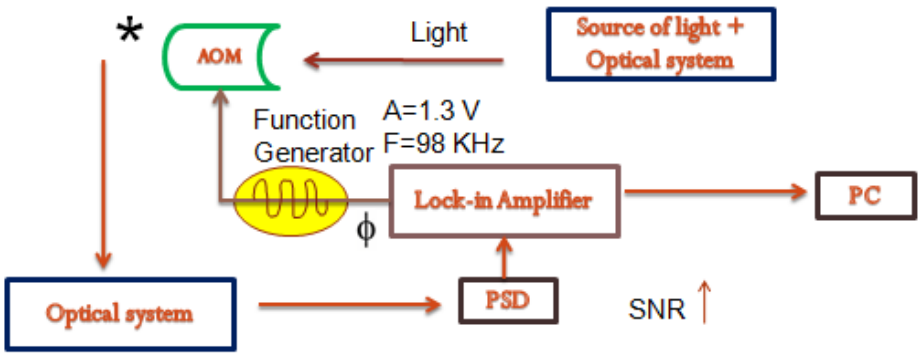

Fig. 9. Block diagram of signals processing in the experiment.

2.6 Pump Probe Technique

The study of energy transport in a nondestructive fashion is possible using a clever and ingenious technique which puts together all the devices and physics described above in a pump probe spectroscopy.

Energy transport can be manifested in changes of reflectivity produced by relaxation of hot carriers, phonons-electrons interaction, scattering processes and thermal coupling between carriers and lattice [27]. Then one can associate refraction index changes as a function of those processes.

It is necessary to have an experiment to measure or characterize such phenomena. Fortunately the pump probe technique is quite adequate to measure reflectivity changes on a picoseconds scale. In fact, this is what we are going to measure. In order to understand such dynamics in silicon on glass sample, such measurement is done by the use of pump and probe beams. In fact those changes are produced by the pump beam which excites

the material generating carriers, producing changes in transmittance and reflectance.

Then the use of a probe beam which allows us to measure such changes, in fact those spectroscopic measurements allows to measure interactions of the generated carriers and relaxation processes.

Typically pump probe techniques are classified as degenerated and non-degenerated, in the first one pump and probe have the same frequency or the same color. In the last one, pump and probe use different frequencies. We show a typical degenerated pump probe setup in the following figure. In order to mention the modifications done in our experiments, we provide an explanation on this typical setup, moreover we show some pictures in appendix E.

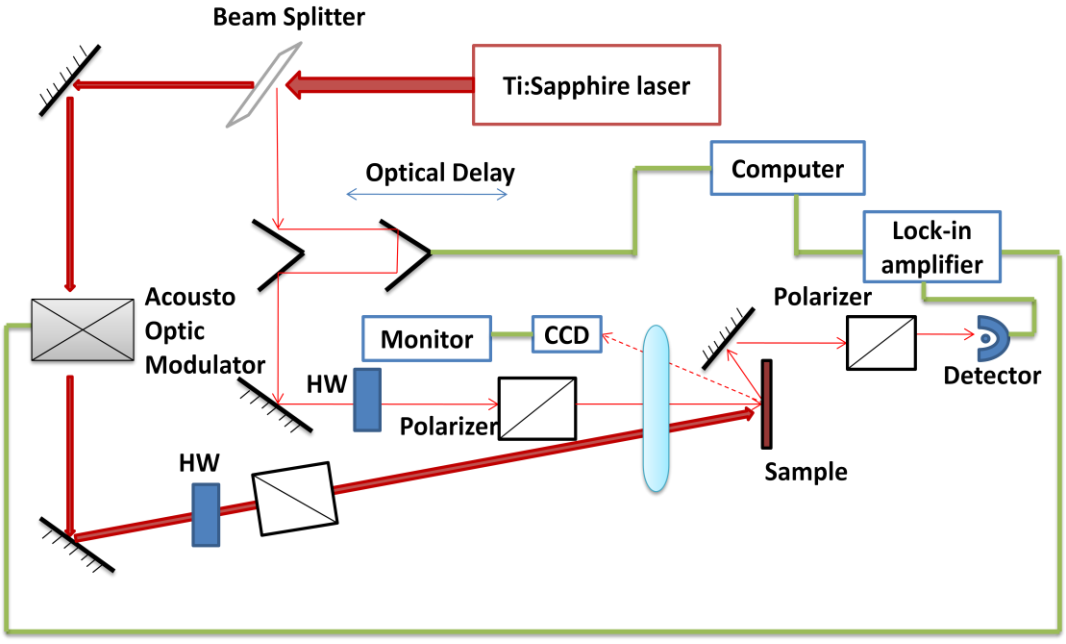

Fig.10 Typical degenerated pump probe setup.

The Pump-Probe technique takes advantage on the nature of the femptosecond lasers. We split the original beam into two beams. Those are

the probe and the pump beams, with an intensity ratio of 1:9. The first one is a low intensity beam and the second is a high intensity beam. The term degenerated comes from this fact that both probe and pump have the same frequencies. The typical reflectance set up is shown in Fig. 10, where we refer to each arm of the setup as the probe and the pump arms respectively. The Pump arm is outlined by a darker red arrow and the beam probe (thinner red) goes through the optical delay electronically interfaced with the detector.

Let us describe the pump arm. The pump beam aims at the sample, but before goes through a mirror and then into an AOM where the signal is modulated in order that the reflected light from the sample becomes detectable by the Lock-in-amplifier. Also, it is important to choose a given orientation of the beam in order to block scattered light onto the detector, arriving from the transmission or the reflection of the pump beam, and to avoid interference effects. For this, we have placed a cross polarizer before the detector, to block the scattered light, reducing the generation of noise on the detector. After the beam acquires certain polarization, with the half wave plate (HW) and the polarizer, the pump signal is ready to excite the material and to generate carriers.

As we have stated, those generated carriers produce ultrafast phenomena that change the optical properties. The way to measure those changes is with the probe beam, which travels along the probe arm. The probe arm has an optical delay module which can be understood as a mobile rectangular retroreflecting prism controlled by a computer.

The computer moves a translational stage that varies the optical path length between the pump and the probe. It is important to mention that it is impossible to obtain any signal, if the pump beam generates carriers and the

probe beam takes more than the time required to achieve equilibrium state, an analog case can be obtained if the probe illuminates the sample earlier.

In review we can conclude that pump beam generates free carriers, and the probe beam gathers the progression of generated phenomena, created by collective phenomena due to carriers interactions in the picoseconds scale.

2.7 Pump probe experimental setup

The experiments, designed and built with the help of the University of Rochester graduates student Jie Zhang and Hiroshi Irie, are shown in the figure 12. All of them are femptosecond pump probe setups, they are an amazing cluster of interesting ideas and physics put together in order to do ultrafast spectroscopy.

In this section, I show the three setups used along this research, before describing them I will point out the objective of each of them. The first one study the carrier dynamics and the last two aim at studying the phonon dynamics in complementary reflection and transmission setups. Through all of them, the pump arm is the only part which has suffered modifications.
The first experiment, showed in figure 12A, was designed to study carrier dynamics. There, the possibility to reach specific energy levels is quite important, and therein the need to use second harmonic generation and the setup becomes nondegenerated.

If we pump on the front (Glass) side, Fig. 3, we can carry on probe reflectance measurements. They are important because they provide information on the carrier dynamics and their influence on reflectivity changes (a detailed treatment is given in chapter 3).

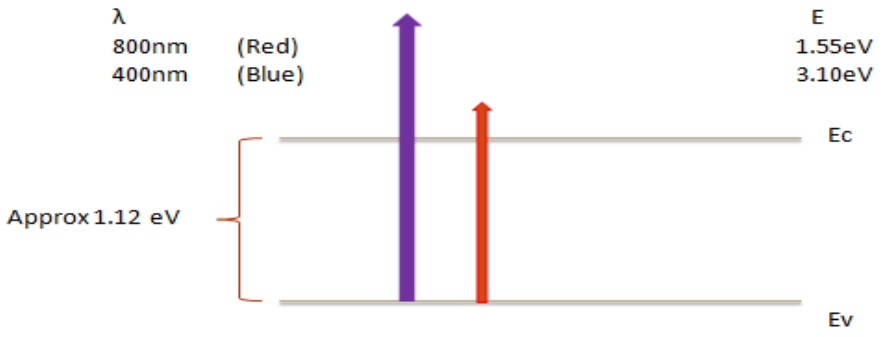

Fig 11. Energy band diagram of silicon on glass sample and the energy of pump and probe beams

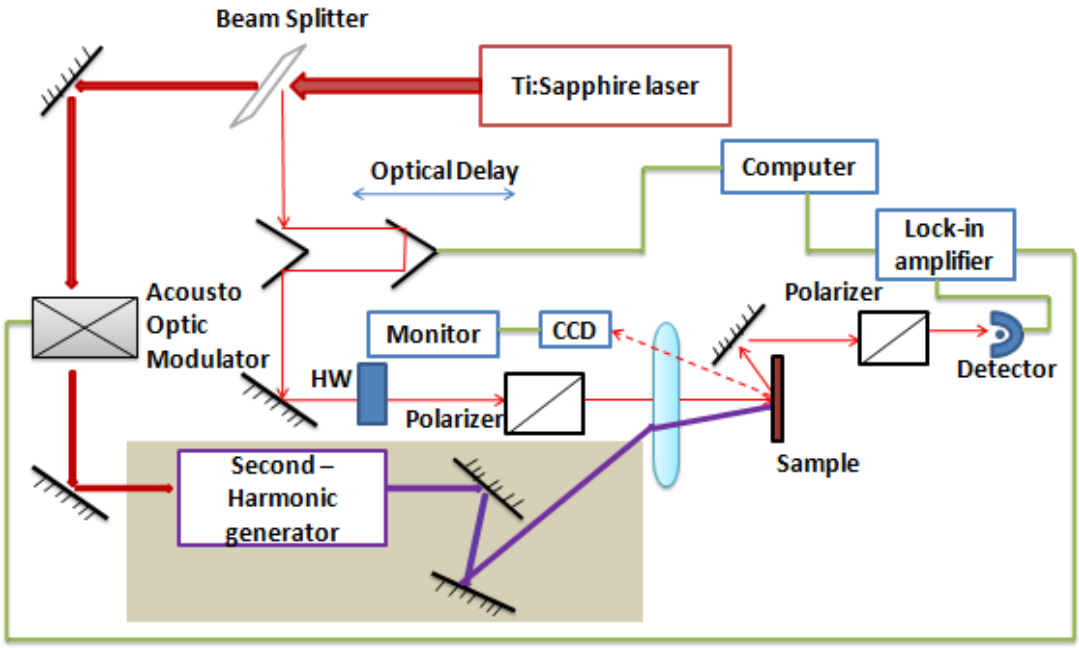

Fig.12A Setup designed to do same side pump-probe reflectance measurement with two colors. This experiment was used in order to study carrier dynamics. (The dark background highlights are modifications done to the experiment shown in Fig 10).

In order to study phonons dynamics, we pump trough a transducer created by a 30 nm Al layer, added on the Si back side of the sample, in order to

improve the thermal expansion and the generation of phonons. This experiment is shown in figure 12B where the pump beam excites the transducer and the response was measured on the other side, trough the probe reflectance. Finally in the last experiment we carry on probe transmittance measurements, Fig. 12C.

The setup described in Figure 12A is a modification of figure 10. The introduction of the second harmonic generator makes unnecessary and replace the half wave plate and the polarizer, because two different wavelengths cannot interfere. In fact this is a non-degenerated pump probe configuration, because pump and probe have different frequencies. But above all, the doubling of frequencies means that we can reach higher energetic levels in the band structures of those materials as shown in figure 11. It is important to mention that second harmonic generation, as well as downconvertion, preserve dispersion relations and satisfy energy and momentum conservation laws. In this process, an ensemble of photons interact with a nonlinear material, if that material allows an addition of frequencies, then such material can be considered as a frequency doubling material and light with the double frequency is obtained.

In this experiment a BBO crystal was used to double the near infrared light of our laser. Then the pump beam has different energy which will allow seeing different steps of the carrier dynamics, and the probe beam works as in the figure 10. The probe arm remains constant as in figure 10, and a parallel polarization was kept, before and after the sample, in order to avoid noise coming from scattering.

The setup shown in figure 12B is used to study phonons dynamics, for that the reason to add a transducer to the sample. The transducer improves the thermal expansion which in turn improves the generation of phonons. Then a

similar reflectance experiment as the one shown in figure 10 is done. The pump light illuminates the transducer film and the propagated phonons are measured on the other side with the reflectance of the probe beam, in fact the mechanism is almost equal to the one described for figure 10, the key differences are on the pump path.

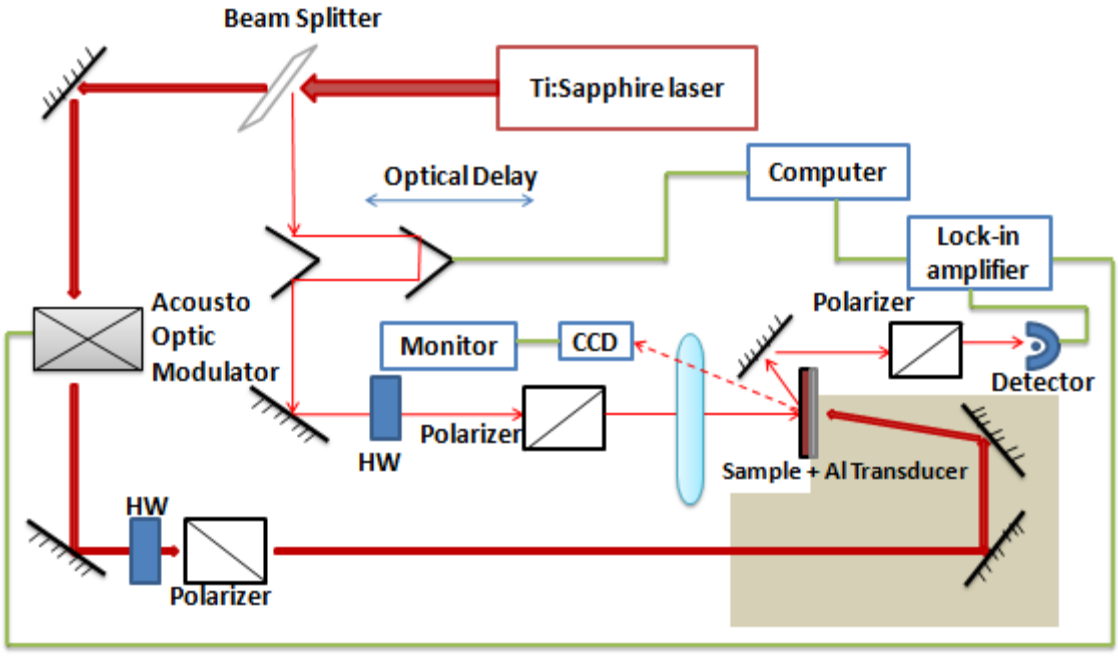

12B. Setup used to do two sides pump probe reflectance measurements with one color. The transducer was added to sample in order to have a good thermal expansion and improve the generation of phonons. (Modifications done to experiment shown in Fig 6 has a dark background).

The setup described in Figure 12C is a transmission analogous to the reflectance experiment described in figure 12B. It proves the reproducibility and consistency of the experiment.

To summarize the previous explanation we make a short review of the experiments done. The three experiments showed in figure 12 have

differences which are consequences in the nature and the physics of the phenomenon under study.

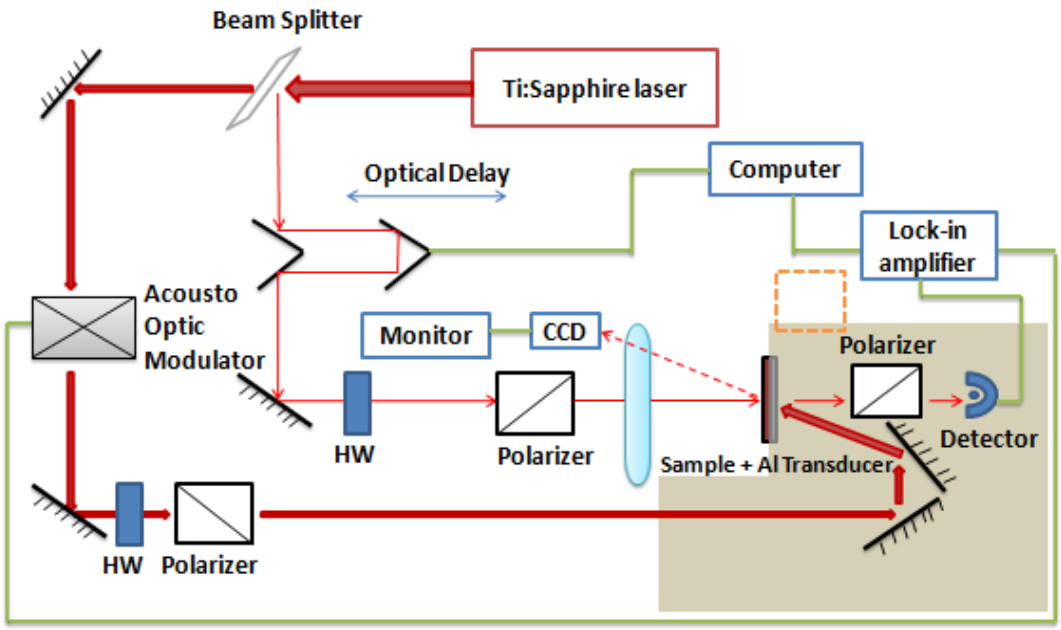

12C Setup built to do two sides pump probe transmittance measurements with one color. This in order to prove the reproducibility of the data obtained in 8B. (Modifications done to experiment shown in Fig 6 has a dark background)

Such differences require different ways to measure transmission and reflectance, as well as the addition of certain optical elements in order to avoid certain undesired phenomena, as well as the way to collect the reflected or transmitted light. In figure 12A two colors are used and both beams illuminate just one side. Then the probe reflected beam is collected, without the need to use a polarizer because the wavelengths are different and they cannot interfere.

In figure 12B, both schemes are used in the probe arm. The same frequency is used for pump and probe, but now the pump is illuminating the

transducer side (the side with the transducer, which was added in order to improve the thermal expansion and the phonons generation, this part will be discussed in chapter 4) As we explained before a carefully orientation of polarizers is needed in order to avoid noise of the sampled signal.

Finally figure 12C uses the same scheme for the pump but now the transmittance is measured. This is done, in order to have a reliable signal and be in a good position to make accurate conclusions as will be described in chapter 4.

Let us discuss the experimental conditions of the sample. As it was explained in chapter 1, the sample has different layers and that generates the possibility of a defective focusing, one spot may be focused in certain layer and another one on a different layer.

The CCD camera helps to achieve a better focusing by taking the focused layer of the sample as a reference, which is not hard to detect. After a focused layer is reached, a process to focus the spots and overlapping is followed.

Typically the spot sizes were around 70 μm and the pump and probe power was modified during the experiments, this information will be provided as results are shown. Finally, the detector shown in all the figures is a Visible DC-125 MHz Low Noise Photodetector, which has as an AC output signal which is send it to a SR830 DSP Lock in amplifier which compares the obtained signal with the signal provided by the function generator which is applied to the AOM.

Chapter 3
Carrier Dynamics

3.1 Abstract

The developments achieved in the field of spectroscopy has allowed scientist to characterize important materials and devices. Pump probe technique has been used to determine ultrafast processes (in the order of femptoseconds and picoseconds) in chemical reactions (i.e. Nobel prize of chemistry 1991) to understand electrical transport, interactions between carriers and lattice, etc. In fact people have found the way to relate the results obtained from pump probe experiments with important and characteristic parameters in the field of interest.

Silicon on glass promises to be a good candidate to develop novel semiconductor device technologies in the field of photonics and electronics. Areas where the lifetime and the mobility of the carriers as well as densities of current, refractiveindex and other more play an important role when a device ought to be designed.

In fact, the reason to describe how and why the results obtained in our pump probe experiment can provide information on carrier processes and how those can be linked with other general parameters.

In this chapter we study the fundamental physical processes that characterize our material. First, we compute the silicon energy bandgap in our

[1] More information about the research that allowed Prof. Amhed H. Zewail to won the Nobel prize can be found in http://nobelprize.org/nobel_prizes/chemistry/laureates/1999/press.html

sample, information that is very important to know in order to simulate and predict devices using SiOG; therefore we propose an easy way to experimentally measure it.

Then we show the results obtained for two SioG samples obtained with different dimensions to be used in our pump probe experiment. We also determined the relaxation and recombination time constants, and their relation with other parameters of material. Furthermore, we study the influence of pump intensity in our measurements.

3.2 Determination of Band Gap Energy in Silicon on Glass sample.

From the theory of semiconductors, it is well known that the energy bandgap of materials is responsible for many interesting physical properties such as the absorption coefficient, mobility of carriers, scattering, conductivity, quantum efficiency, etc [28]. All of them produced by changes in the electronic states in the energy bands.

It is well known that due to size effects [29], properties of bulk materials are completely different from those of thin film materials. Therein the need to determine certain constants parameters such as the band gap energy of the silicon on glass sample. There are other methods of proven capability, Jurgen W. Precker et al [30] and G. P. Joshi, et al [31], but this is convenient for its simplicity and effectiveness.

All the semiconductor materials have different responses to different frequencies of light and this process depends on the band gap energy value of each material. The light energy is given by E= hv and the band gap energy has a given energy value. Here we can distinguish two cases:

If the light excitation frequency is smaller than Ec-Ev, in other words if it is smaller than the energy bandgap, the energy is not enough to cause electron-hole generation. Then the material is transparent or optically inactive to such specific wavelength.

If the energy of the light is quite similar or larger than the energy bandgap, it can produce electron hole generation and carrier movements and the light can be absorbed. In fact that behavior is shown in figure 13.

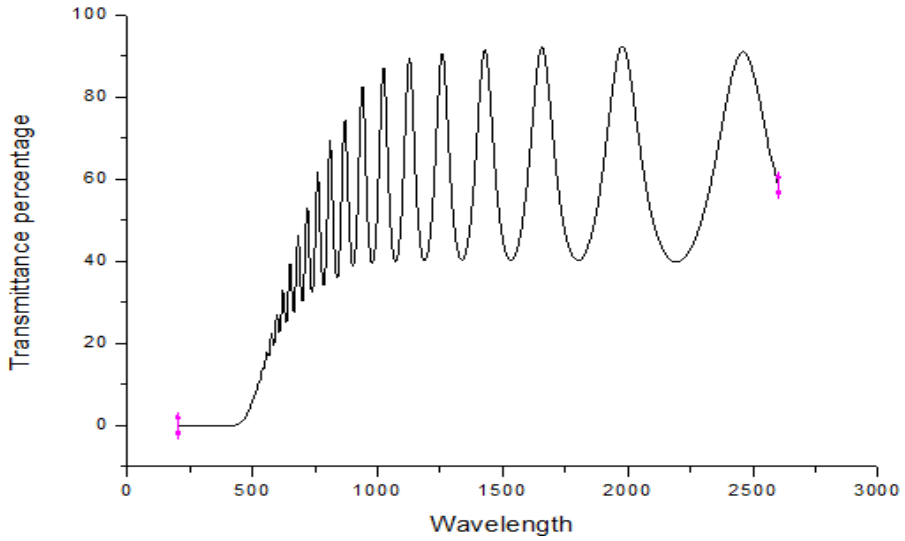

Fig 13.- Transmittance measurements done with a Perkin-Elmer ambda 900 spectrophotometer at the University of Rochester.

Figure 13 shows transmittance measurements done using a Perkin-Elmer Lambda 900 spectrophotometer. Such spectrophotometer, as shown in figure 13, measures the transmitted intensity trough the sample. The frequency of the light is changing along the scanning process; in fact is accompanied by an interference pattern. Nevertheless it is evident that the transmittance percentage is changing, and taking into account the ideas

about bandgaps, one can assume that the energy will be strongly absorbed near the bandgap, and then the transmittance will decrease.

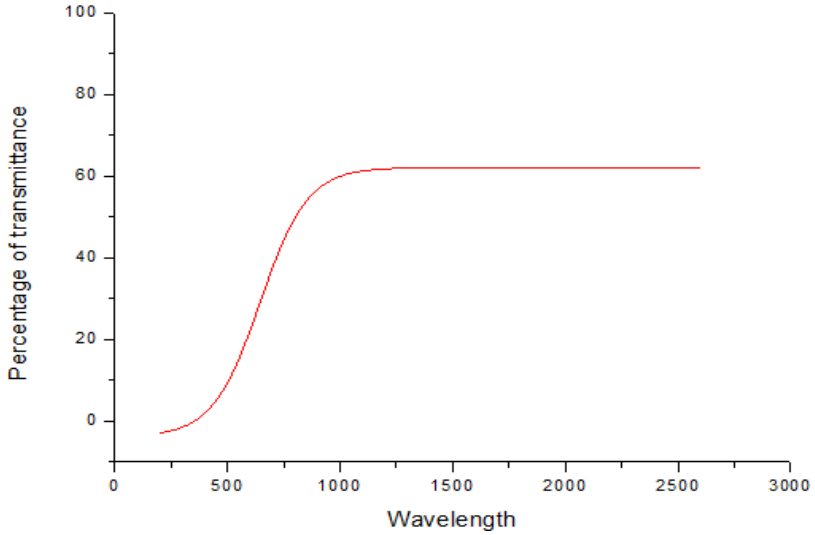

Fig 14.- An average of the transmittance percentage is shown in figure 13

In figure 14 we have adjusted figure 13 to an analytic curve. The slope of the curve is not narrow enough to make a reasonable estimation on the wavelength where the material exhibits the strongest absorption.

For that, the need to find the inflexion point in order to localize the energy associated with such wavelength. There we find the point where its value is null and corresponds to a wavelength of 1119.16 nm, and a band gap energy of 1.106 eV, which is quite similar to the energy bandgap of the typical silicon which is reported as 1.12 eV [32]. This fact shows the efficiency of our proposed method which is simpler than other reported methods used to measure bandgaps of semiconductors

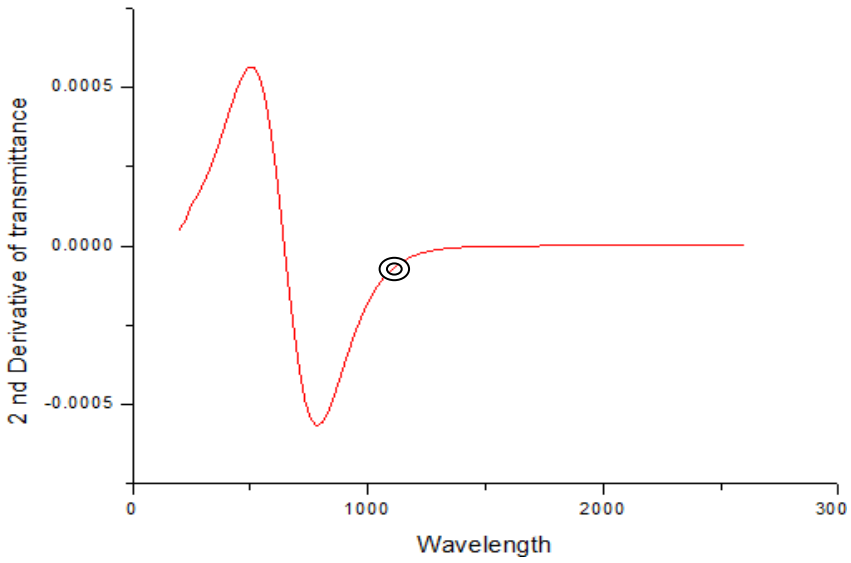

Fig15.- Second derivative of the average of percentage of transmittance.

As we previously stated, the need to be able to draw an accurate picture of different semiconductor phenomena is important and it becomes fundamental when a semiconductor device is planned to be designed, and the band gap energy is probably the most fundamental parameter of a semiconductor.

As it will be shown in this chapter it also has influence in time relaxation and recombination constants.

3.3 Pump probe response and implications.

One of the most important contributions of this thesis is to describe the direct relation between the carriers dynamics and the reflectance, obtained experimentally, and from the last one, the sample characteristics.

The silicon carriers dynamics can be experimentally studied trough the reflection experiment described in the figure 12a of chapter 2 and the results will be described in Fig. 16.

The kinetic energy of the excitation field, which is higher than that of the lattice, and the unbounded electrons or mobile electrons or holes in the conduction and balance bands respectively [33], cause the very fast physical process of the generation of hot carriers and currents.

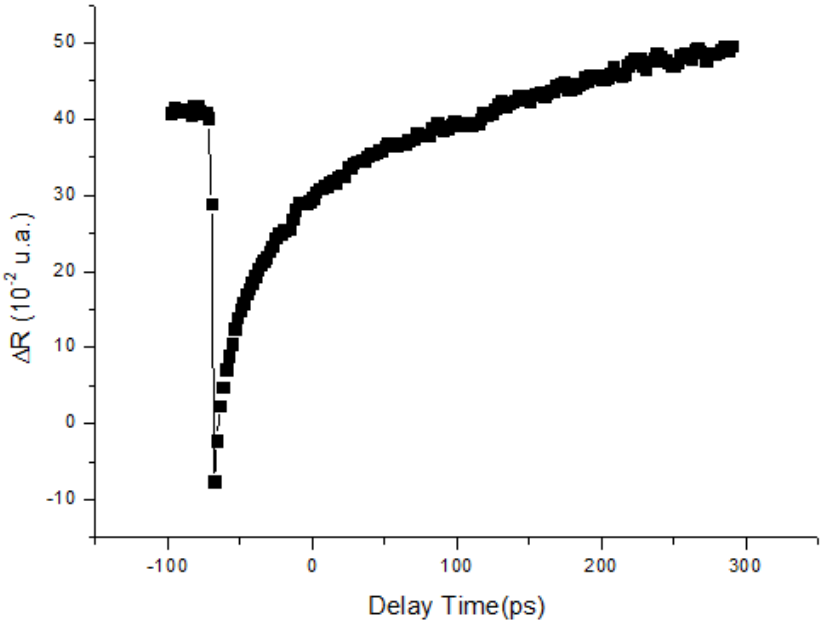

Fig 16.- Pump probe reflectance measurements for 1.43 um sample.

The experiment shows great ingenuity from its initial conditions. We assure ourselves that both pump and probe are focused on the same spot, of the order of 70 um, on the same silicon layer. The essence of the experiment is to produce a delay between pump and probe trough the motion of a delay station that swept on a 400 ps range in our experiment.

In fact, we define as ∆R the reflectance difference between the probe beam reflectance with and that without the pump beam. Figure 16 shows

changes in the reflectance on a picoseconds scale, showing the capability of the technique.

The sharpest depth (valley) was obtained when both pump and probe traveled the same optical path length. In our plot that corresponds to minus 67 ps, that expressed in distance means that the optical delay station was already close to 10 cms (half of 67ps times c) from its initial position to obtain an equal optical path. At that moment, the equilibrium state of silicon was broken, and hot carriers were generated [34], producing changes in reflectance, as shown in fig 16.

Furthermore, it is easy to realize the reflectance difference measured before and after the pump probe peak. Before that peak the reflectance was constant, that means a carriers equilibrium state, and after the peak was obtained a curve formed by two different exponentials, as we will shown below. The dependence on other physical variables was also explored on similar experimental realization and similar plots were obtained, to the one showed in figure 16, after scanning on those ranges.

An analysis of the carrier dynamics from first principles allows us to establish the desired relation to understand the reflectance behavior. Before continuing it is important to point out the assumptions made in order to use this description.

- The first is that in general the number of carriers is quite large η
- Each one of the carriers satisfy its corresponding Schrödinger equation with wave equation ψ_n , such that:
  - $\int |\psi_n|^2 dx^3 = 1.$ (5)

- The general behavior of the carriers can be modeled by an ensemble defined by

$$\Psi = \sum_n a_n \psi_n. \tag{6}$$

Which also satisfy the collective Schrodinger equation, but such that the total number of carriers is given by:

$$\eta = \int |\Psi|^2 dx^3 = \int N dx^3. \tag{7}$$

Where $$N \sim |\Psi|^2 = \Psi\Psi^*. \tag{8}$$

is the density of electrons or holes (carriers) in each point [35],

Now that we know the carrier generation is the responsible of such reflectance changes, we aim at modeling its density of carriers N. Therefore we will obtain its corresponding continuity equation. We can think in a ensemble of carriers described by a collective Schrödinger equation, with a function of excitation given by (t) , that describe sinks or sources and therefore is accompanied by i. In case that $\mathbb{I}(\mathrm{t})$ is positive, such function can be understood as a source of carriers, which is the responsible to plays the role of source of excitation, then the following equation can be written as:

$$i\hbar \frac{\partial \Psi}{\partial \mathrm{t}} = -\frac{\hbar^2}{2\mathrm{m}} \nabla^2 \Psi + (V + i\mathbb{I}(\mathrm{t}))\Psi. \tag{9}$$

A convenient expression to obtain the density of carriers is $\mathrm{N} = \Psi\Psi^*$ then we write the conjugated equation,

$$-i\hbar \frac{\partial \Psi^*}{\partial \mathrm{t}} = -\frac{\hbar^2}{2\mathrm{m}} \nabla^2 \Psi^* + (V - i\mathbb{I}(\mathrm{t}))\Psi^*. \tag{10}$$

After multiplying the first by Ψ^* and the second by Ψ, the following equations are obtained:

$$i\hbar\Psi^*\frac{\partial\Psi}{\partial t} = -\frac{\hbar^2}{2m}\Psi^*\nabla^2\Psi + (V + i\mathbb{I}(t))\Psi^*\Psi. \quad (11)$$

$$-i\hbar\Psi\frac{\partial\Psi^*}{\partial t} = -\frac{\hbar^2}{2m}\Psi\nabla^2\Psi^* + (V - i\mathbb{I}(t))\Psi\Psi^*. \quad (12)$$

After subtracting the previews equations, is easy to obtain the following expression.

$$\Psi^*\frac{\partial\Psi}{\partial t} + \Psi\frac{\partial\Psi^*}{\partial t} = \frac{i\hbar}{2m}(\Psi^*\nabla^2\Psi + (V + i\mathbb{I}(t))\Psi^*\Psi - \Psi\nabla^2\Psi^* - (V - i\mathbb{I}(t))\Psi\Psi^*). \quad (13)$$

And reordering;

$$\Psi^*\frac{\partial\Psi}{\partial t} + \Psi\frac{\partial\Psi^*}{\partial t} = \frac{i\hbar}{2m}(\Psi^*\nabla^2\Psi - \Psi\nabla^2\Psi^* + 2i\mathbb{I}(t)\Psi^*\Psi). \quad (14)$$

$$\Psi^*\frac{\partial\Psi}{\partial t} + \Psi\frac{\partial\Psi^*}{\partial t} = -\frac{i\hbar}{2m}\nabla\cdot(\Psi\nabla\Psi^* - \Psi^*\nabla\Psi) - \frac{\hbar}{m}\mathbb{I}(t)\Psi^*\Psi. \quad (15)$$

As we previously stated, we are modeling the behavior of an ensemble of particles with a collective Schrödinger equation, then we can use the expression given by (8) for the density of particles. This allows to write the left part of equation (15) as $\frac{\partial N}{\partial t}$, which represents the changes of the carriers density with the time, in fact Eq. (15) has already all the form of a continuity equation [36],

$$\frac{\partial N}{\partial t} = -\nabla\cdot\vec{J} + G(x_i, x_j, x_k, t). \quad (16)$$

In fact (16) allows describing changes on carrier density with time, where $\vec{J}=\frac{i\hbar}{2m}(\Psi\nabla\Psi^{*}-\Psi^{*}\nabla\Psi)$. We could relate these specific elements with observables:

It is well known that $\vec{J}=\vec{v}N$, and after applying some vector identification we obtain:

$$v=\frac{i\hbar}{2m}\left(\frac{\nabla\Psi^{*}}{\Psi^{*}}-\frac{\nabla\Psi}{\Psi}\right). \tag{17}$$

which is the drift velocity $\vec{v}_d$ in the silicon, which is also proportional to the carrier mobility $\vec{v}_d=\mu\vec{E}$. Here μ is the carrier mobility and $\vec{E}$ is the electric field.

Additional information on the conductivity can be obtained using the constitutive relation, $\vec{J}=\sigma\cdot\vec{E}$ where σ is the conductivity tensor. This is an important point; we have also modifications in the conduction properties.

However, the most important relation for our experimental analysis is to realize that the carrier dynamics correspond to a change in the refractive index. Then using the Drude model [37] and a power expansion, it is easy to obtain the following expression for refraction index changes due to the carriers density,

$$\Delta n=\frac{\Delta N e^{2}}{2\epsilon_0 m^{*}(\omega_0^{2}-\omega^{2})}. \tag{18}$$

That relates the refractiveindex change and that of the density of carriers ΔN, generated by the pump excitation. There e is the electron charge, ϵ_0 is the permittivity in vacuum, m^{*} is the effective mass of electrons and holes, ω_0^{2} is the resonance frequency and ω^{2} is the frequency of the excitation light.

As consequence, one the most important relation for this thesis is the one that relates those variations of refractive index with the reflectance changes. That is the well known relation between the reflectance (at normal incidence), including the absorption part, and given by [38]:

$$R = \frac{(n-1)^2+k^2}{(n+1)^2+k^2}. \tag{19}$$

where n is the real part of refraction index and k is its imaginary or absorption part. On the other hand, from elipsometry measurements done by D.E Aspnes et al [39], it is known that the silicon permittivity is given by $\epsilon = 13.656 + 0.048\, i$.

Therefore for our purposes, we can neglect the imaginary or absorption part k in Eq. (5) because is very small compared with the real part, and for that is enough that k is smaller that n and $(n-1)$.

This is quite a general and convenient relation for the specific conditions of our experiment, if we realize that the pump probe experiment has resulted in a refractive index change. Therefore, the detailed reflectance variations ΔR, with and without an excitation pulse, can be written as follow:

$$\Delta R = \frac{\left(n+\Delta n\left[I_{pump}(t),I_{probe}(t)\right]-1\right)^2}{\left(n+\Delta n\left[I_{pump}(t),I_{probe}(t)\right]+1\right)^2} - \frac{(n-1)^2}{(n+1)^2} \sim \frac{4n}{(n+1)^3}\Delta n\left[I_{pump}(t), I_{probe}(t)\right]. \tag{20}$$

Where $\mathrm{I_{pump}(t)}$ and $\mathrm{I_{probe}(t)}$ are the pump and probe intensities with a time dependence. In fact $\Delta \mathrm{n}\left[\mathrm{I_{pump}(t), I_{probe}(t)}\right]$ has a similar behavior to $\Delta \mathrm{R}$, except for a constant, and both are functions of pump and probe intensities and time.

Finally, let us refer to the subject matter. The transient processes, those can be thoroughly studied from first principles and from experimental evidence. From the later, it is clear that we could describe the problem in characteristic times τ_k. In fact, two processes are fundamental to our problem, relaxation and recombination of carriers characterized by the times τ_{Rx} and τ_{Rb} respectively, and those constants are closely related with the energy of carriers in electronic bands. The relaxation describes the carriers scattering processes and cooling processes by emission of optical phonons, while the recombination describes the recombination of holes and electrons produced by different mechanisms.

There is an excellent and suitable derivation of the relaxation time given by Manuel Cardona in his classical book [40]. The transient mechanism acts on the carrier distribution, whose steady state condition is given by the Fermi-Dirac distribution [41] described by:

$$f_k^0 = \frac{1}{e^{\frac{E_k - \mu_F}{k_B T}} + 1}. \tag{21}$$

Where μ_F is the Fermi energy k_B is the Boltzmann constant and T is the temperature in the absolute scale. He associates the time changes of the carrier distribution with the applied field effects and the scattering of the carriers:

$$\frac{df_k}{dt} = \left(\frac{\partial f_k}{\partial t}\right)_{field} + \left(\frac{\partial f_k}{\partial t}\right)_{scatt}. \tag{22}$$

If we consider the applied field $\vec{E}$ small enough and comparing the carriers dimensions with the wavelength of our field we consider the field as constant in time therefore the distribution is also a constant in time, then it is possible to expand f_k around f_k^0 as a function of $\vec{E}$.

$$f_k = f_k^0 + g_{Rx}(\vec{E}). \tag{23}$$

We assume that scattering processes is going to cause g_{Rx} to relax with a time constant τ_{Rx}.

$$\frac{df_k}{dt} = \left(\frac{\partial f_k}{\partial t}\right)_{field} - \frac{g_{Rx}}{\tau_{Rx}}. \tag{24}$$

And the field term can be written using the chain rule as:

$$\left(\frac{\partial f_k}{\partial t}\right)_{field} \approx \left(\frac{\partial f_k^0}{\partial E_k}\right)\left(\frac{\partial E_k}{\partial t}\right) = \left(\frac{\partial f_k^0}{\partial E_k}\right) q\overrightarrow{v_k} \cdot \vec{E}. \tag{25}$$

Where $\overrightarrow{v_k}$ is the carriers velocity. Then here we assume that scattering processes is going to cause g_{Rx} to relax with a time constant τ_{Rx}. Then substituting (23) and (25) in (24) we can obtain an expression for the relaxation constant as follow.

$$\tau_{Rx} = g_{Rx}\left(\frac{\partial f_k^0}{\partial E_k}\right)^{-1}\left(q\overrightarrow{v_k} \cdot \vec{E}\right)^{-1}. \tag{26}$$

On the other hand, the recombination process can occur for different mechanisms. The indirect mechanism uses the traps or defects in the semiconductor [42], like dislocations or lattice imperfection. In fact, those imperfections acts as a recombination centers which has the capability to trap holes and electrons, then the probability of recombination increases. Then the recombination time is proportional to the concentration of holes p_0 and electrons n_0 as follow $\tau_{Rb} = g_{Rb} n_0\ p_0$.

Once that material characteristics have been defined and their relation with the reflectance, described by Eqs (20), (18) and (16). We can carry on the transient analysis of our experiment. In expression 18, we showed that changes in refractive index were proportional to changes in carriers density, then refractive index changes are proportional to changes in reflectance. This part allows us to rewrite (16) as:

$$\frac{\partial \Delta R}{\partial t} + \vec{\nabla} \cdot (\overrightarrow{\mathrm{v_d}} \Delta R) = \mathrm{C_1 G}(\mathrm{x_i}, \mathrm{x_j}, \mathrm{x_k}, t). \tag{27}$$

Where $\mathrm{C_1} = \frac{\mathrm{e}^2}{\epsilon_0 \mathrm{m}^*(\omega_0^2 - \omega^2)} \frac{2\mathrm{n}}{(\mathrm{n}+1)^2}$ is a constant that contain the constant factors given in Eqs, (18) and (20). It is well known that the drift velocity $\mathrm{v_d}$ is the steady-state velocity of a charge. If we assume that the reflectivity is mostly constant with position and $\mathrm{v_d}$ is nearly a constant, then Eq. (22) can be rewritten as:

$$\frac{\partial \Delta R}{\partial t} + \mathrm{C_0} \frac{\Delta R}{\tau_c} = \mathrm{C_1 G}(\mathrm{x_i}, \mathrm{x_j}, \mathrm{x_k}, t). \tag{28}$$

Where $\mathrm{C_0} = \vec{\nabla} \cdot \vec{\mathrm{r}}$ and $\vec{\mathrm{r}}$ is a position vector.

We can model our excitation beam by a Gaussian form given by $\mathrm{G}(\mathrm{x_i}, \mathrm{x_j}, \mathrm{x_k}, t) = \mathrm{I}(\mathrm{x_i}, \mathrm{x_j}, \mathrm{x_k}, t) = \mathrm{I}(t) = \mathrm{I_0 e}^{-4\ln 2 \frac{\mathrm{t}^2}{\tau_p^2}}$, where τ_P is the pulse duration. If we solve equation (28) with such excitation beam, one can obtain the following expression for reflectance:

$$\Delta R = A e^{\frac{t}{\tau_p}} + \frac{1}{4} \mathrm{e}^{\frac{\tau_\mathrm{P}^2}{\mathrm{Log}[65536]\tau_\mathrm{c}^2} - \frac{\mathrm{t}}{\tau_\mathrm{c}}} \mathrm{Erf}\left[\frac{2t\sqrt{Log[2]}}{\tau_P} - \frac{\tau_P}{4\sqrt{Log[2]}\tau_c}\right] \sqrt{\frac{\pi}{Log[2]}} i_0 \tau_P \,. \tag{29}$$

That can be rewritten as:

$$\Delta R = A(t)e^{-\frac{t}{\tau_{Rx}}} + \mathrm{B(t)e}^{-\frac{t}{\tau_{Rb}}} . \quad (30)$$

This means that we can fit the obtained plots with a function with the same form as (30). In fact the effectiveness, of such result is shown in the following figure.

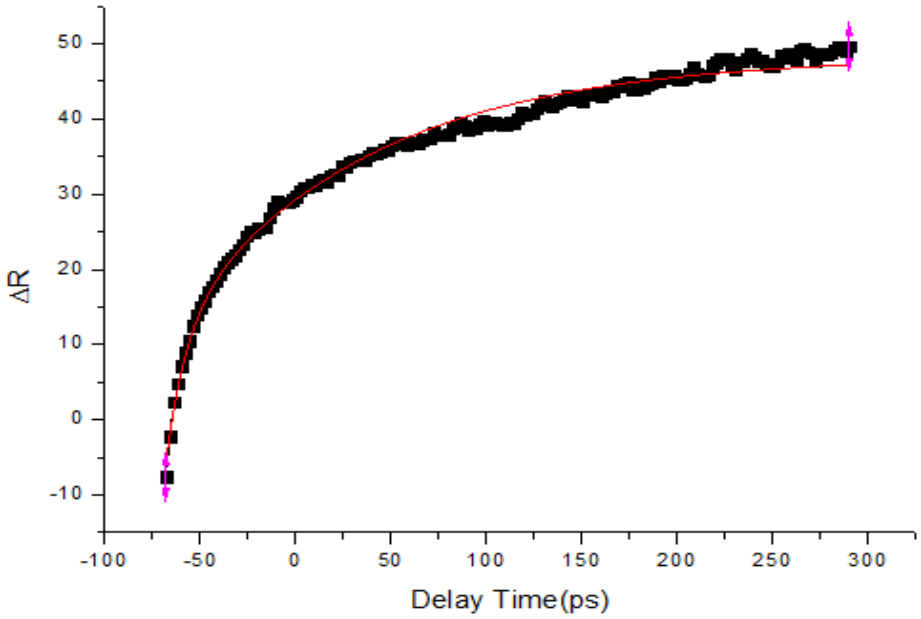

Fig 17- Fitting of pump probe reflectance measurements using equation 21

It is clear the excellent agreement between the experimental data and our theoretical assumptions. In fact such fitting has a physical meaning that we can relate with native processes in the material. In fact we associate them with the relaxation time and recombination time, and as we stated in chapter 1, the first is a very fast process and the second is very slow.

Once that the theoretical background of our experimental results have been developed we are in a good position to develop a picture of different behaviors in our sample. In fact those time constants allows to know other

parameters of a semiconductors, and we after the fitting part was done we will know the numerical value of such constants.

In this thesis we determined this constant using equation (30) to fit the plot showed in figure 17, the obtained value as 10.36 ps for recombination constant and 103.25 ps for recombination constant, which are the expected range for that value.

Now we can rewrite equation (30) as follow:

$$\Delta R = A(t)\, e^{-\frac{\left(\frac{\partial f_k^0}{\partial E_k}\right)(q\vec{v_k}\cdot\vec{E})}{g_{Rx}}t} + \mathrm{B(t)}\, \mathrm{e}^{-\frac{\mathrm{t}}{g_{Rb} n_0\ p_0}}. \quad (31)$$

Equation (31) is an interesting expression that relates changes in reflectance with changes in the Boltzmann function with the energy of carriers, the velocity of carriers, electric field and concentration of holes and electrons. By that, the importance of this time constants, they enclose many interesting parameters that can be obtained from such constants, in fact those constants are characteristic parameters of materials that provide the opportunity to characterize semiconductors.

Once that we determined the relaxation and recombination time constants which are the fundamental results of this chapter, the following was to study the influence of intensity in excitation of carriers, in case to have some influence this should be related in time constants, as we previously explained many important parameters converge in the time constants. After measuring at different pump intensities we obtained the following plot.

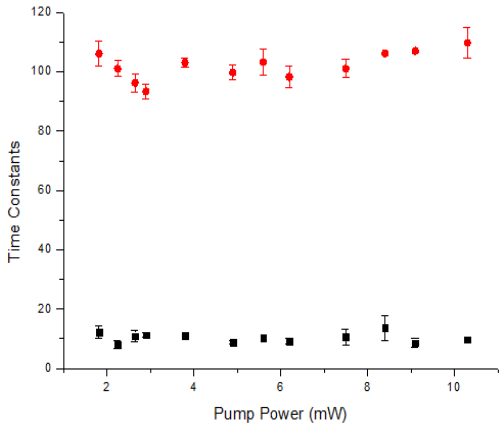

Fig 18.- Time constants variation with pump beam intensity, red line represents recombination time and black line represents relaxation times.

Figure 18 shows that there is not influence from intensity variations with the recombination process and the relaxation step. All those measurements were done in the sample with a thickness of 1.43 um.

Then is important to be aware that carriers as an ensemble of particles have different behaviors depending on the medium and the magnitude of such mediums [43], different behaviors are produced. In the other hand, when photonic and electronic devices are designed, the need to miniaturize the device always exists [44], therein the reason to study that behavior in a 200 nm sample, after pump probe experiment was applied to this sample the next plot was obtained:

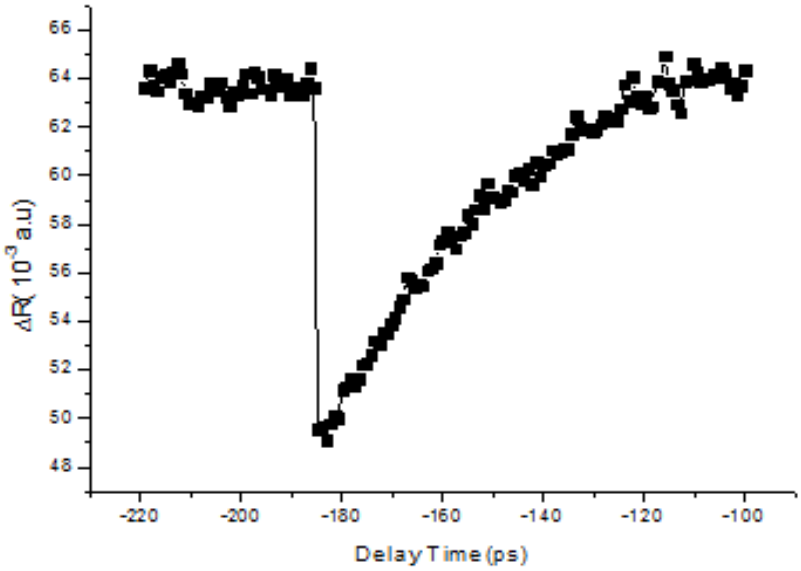

Fig19.- Pump probe reflectance measurements for 200 nm sample.

Figure 19 shows slightly differences in the curvature after the pump probe signal, this means, differences in the relaxation and recombination times, in fact after the fitting was done, using eq. 21 the following plot was obtained

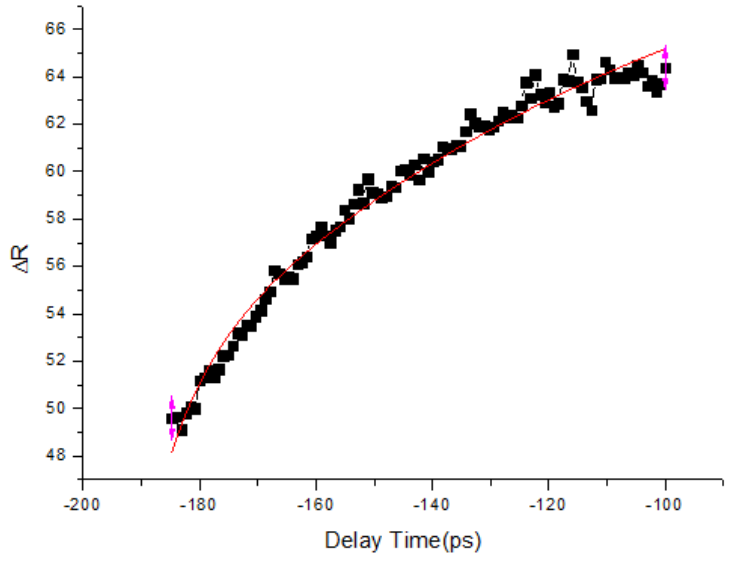

.

Fig 20 -Fitting of pump probe reflectance measurements in 200 nm sample using equation 21.

The value for time constants, after the pump power was tuned is shown in the next picture:

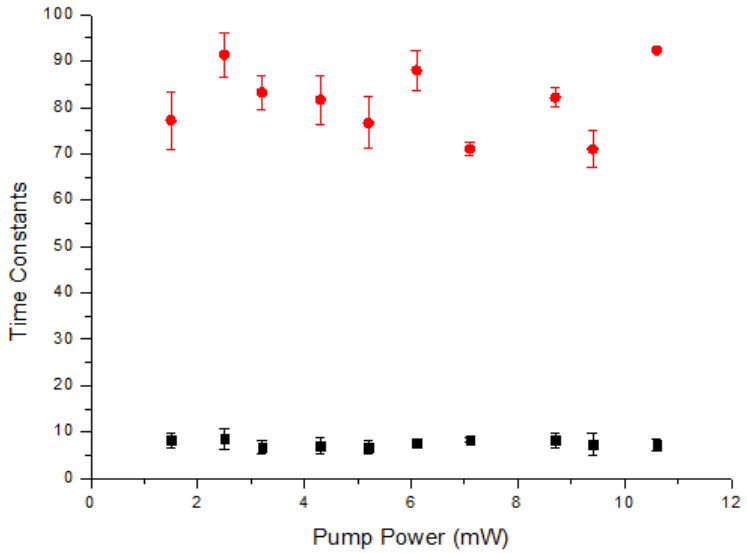

Fig 21.- Time constants variation with pump beam intensity for 200 nm sample, red line represents recombination time and black line represents relaxation times.

As can be seen from figure 21, there are not a clear tendency when the pump beam changes. Moreover the figure 21 has different value for time constants than figure 18, but such difference is very small, then the parameters that determine such time constants do not vary drastically with the sample neither with the intensity used. The above results position in this material as a good prospect to develop semiconductor devices [45].

Chapter 4

Generation and detection of phonons and their dynamic properties.

4.1 Abstract

This chapter shows one of the most interesting experimental results obtained in this research project. In fact, our experimental results are quite unusual and the proposal for our theoretical explanation regards in the propagation of a phonon wave packet, which evolves in space and time with a finite spectrum and that is quite unusual and important because its implications. Moreover we provide a proposal of the finite spectrum that demonstrate that such behavior is a consequence of the temperature.

Furthermore the physics used to explain the obtained results is quite interesting and because the educational profile of students in optics department we have considered convenient to provide a review of the basics of the phonons theory.

Such review consists on explaining the difference of phonons oscillations with other kinds of waves, this will allow understanding the behavior and possible phenomena that phonons can suffered, the environment or the

nature of the excitations that phonons need in order to be created and transported.

In this part of research we needed to add a transducer in order to achieve a good thermal expansion, we explain the influence of such transducer, as well as a positive step that we observed in our pump-probe measurements after the transducer was added.

4.2 Theoretical background of phonons

In order to establish a clear understanding of the phenomenon under study it is convenient to provide a definition of phonons; they are defined as elementary quantum of vibrational energy of the atoms in the crystal [46]. They are usually generated by electrical or optical perturbations which act as a Planck source of heat. In fact such perturbation generates hot carriers, which will achieve an equilibrium state in different steps, as we explained in chapter 1.

Those carriers steps and heat transport are characterized for momentum conservation. Moreover at low temperatures, near to 0 K, the used heat pulse to generate phonons that travels in the crystalline material without scattering and manifest a ballistic behavior [47]. That is quite different to the phonon propagation at room temperature, where scattering between phonons is strong and reduce the phonon lifetime.

Once we have provided a definition of the phonon, it is clear that we have a problem of wave physics with all its implications. First we need to clarify up that exists different kind of waves, transverse waves and longitudinal waves. In the first the displacements or oscillations in the medium are transverse to the direction of propagation. In the second one, oscillation motion is in the

same direction as the wave propagation and both of them are solutions to the wave equation. In this thesis we study acoustic phonons and its branch contains 3 modes; one longitudinal and two with transverses. The transverse modes can be divided in fast and slow transverse and we study just the longitudinal mode.

Another characteristic of the wave is its velocity; in fact there are different velocities, therein the need to briefly describe the three different types:

- Signal velocity: This is the velocity of the oscillator about its equilibrium position.
- Phase Velocity: Is the velocity that describes the change of position in the time of determined wave-front in the oscillations.
- Group Velocity: When the wave under study is described using more than one harmonic, it may be superposed and form a group characterized by a Group velocity. However, each one of the components will travel at different velocities causing dispersion of the group.

In order to be able to explain in a mathematical form the difference between phase and group velocity is convenient to consider the next mechanical system of masses in order to obtain a dispersion relation:

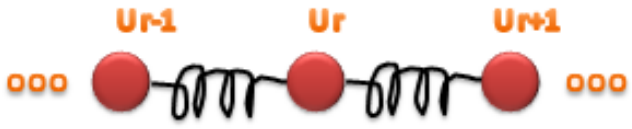

Fig. 22 Linear chain model used to explain dispersion of phonons

In the figure above we model the lattice of a non-polar material with an atom per unit cell which is quite different to silicon which has 8 atoms per unit cell [48], in spite of that, this model is good enough to point out the difference

between phase and group velocity. A rigorous formulation of dispersion relation for silicon was done by Rana Biswas and Vinay Ambegaokar [49].

A force analysis of the mass and springs systems shown in figure 22, allow us to obtain the following expression

$$m\frac{\partial^2 u_r}{\partial t^2} = \alpha\left[\left(u_{r+1}-u_r\right)-\left(u_r-u_{r-1}\right)\right] = \alpha\left[u_{r+1}-2u_r+u_{r-1}\right]. \qquad (32)$$

where u_r is the displacement of the atom, m is the mass of the atom, and α is the force constant of the spring. The solution u_r of this equation is given by $u_r = u_0{}^r e^{i(rka-\omega t)}$, where $u_0{}^r$ is the amplitude of vibration of the r[th] mode, k is the wavevector and ω is the angular frequency. If we assume equal amplitudes and if we substitute in equation (32) we can obtain the following dispersion relation:

$$\omega^2 = \frac{2\alpha}{m}(1-Coska). \qquad (33)$$

Furthermore, the phase velocity is defined by $\frac{\Delta\omega}{\Delta k}$, and group velocity by $\frac{d\omega}{dk}$.

We can notice the nonlinearity in expression (33) and see that if the wavevectors are chosen in a nonlinear region of the dispersion curve is clear that phase velocity is not equal to group velocity, In fact the dispersion relation obtained by Biswas and Ambegaokar [49] is not linear.

4.3 Elastic Continuum Model of Phonons

It is important to mention that typically most of the experiments, where sound velocity corresponds to the time of flight of the heat pulse, are

conducted in a non-dispersive frequency conditions, and our theoretical model is based on the scattering of wave packets [50].

In fact we will be using the last definitions in order to explain the physics behind our phonons phenomena. Before continuing with our research results we will talk about the nature of phonons.

We can start thinking in arbitrary arrangements of atoms, in fact they can be the same atom or different atoms, the physics will be the same. In fact we can use the elastic continuum description or the linear chain model, as we did it to obtain a dispersion relation, for convenience people usually uses the first to obtain a mathematic model for the behavior of phonons and the second to obtain a dispersion relation [51].

Typically longitudinal acoustic phonons are modeled with the elastic continuum model. In order to develop such model, it is convenient to define certain key concepts that will allow linking the elasticity module (E) with the force by the following expression

$$F = AE\frac{\partial^2 u}{\partial z^2}. \tag{34}$$

Furthermore it is important to say that stress quantifies how a solid is distorted from its original shape; in fact we can consider changes in stress as follow

$$\sigma = E\frac{\partial u}{\partial z}. \tag{35}$$

In addition it is convenient to introduce the elastic strain parameter that can be defined as follow

$$\eta = \frac{\partial u}{\partial z}. \tag{36}$$

Moreover we can start considering a dx element, as it is shown in the following picture.

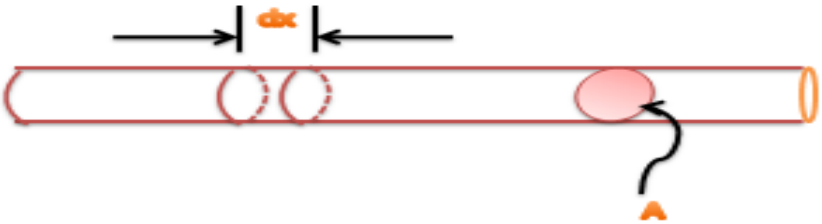

Fig 23. Elastic continuum model of phonons, used to explain its relation with strain and stress

Then we can apply the second Newton's law as follow

$$dm\frac{\partial^2 u}{\partial t^2} = F. \tag{37}$$

where u is the linear displacement, the differential element of mass is given by $dm = \rho A dx$, where ρ is the volume density, *A* is the transversal section of area and dx differential displacement. Using the previous definition of force one can obtain the following model

$$E\frac{\partial^2 u}{\partial z^2} = \rho\frac{\partial^2 u}{\partial t^2}. \tag{38}$$

In addition, we can rewrite it as follow

$$\frac{\partial \sigma}{\partial z} = \rho\frac{\partial^2 u}{\partial t^2}. \tag{39}$$

Once that we have formulated a general model for phonons. We are now interesting to know how such mechanical perturbation can be detected by our experimental setup, here we provide the ideas.

As we stated in chapter 3, the generation of hot carriers induces changes in refraction index, then those hot carriers transfer their excess of momentum

to the lattice generating acoustic phonons, which introduce changes in material such as stress that also contribute to changes in refraction index.

This means that in order to ensure that the strong phenomenon is due to phonons or carriers, the signal will need to be isolated as we will show it later. Then one can generalize the preview linear description to a real description with complex geometries by the use of tensor formalism. Then using important results provided by Thomsen *et al* [52] that relates the generated electrons with changes in stress as

$$\eta = \frac{\partial E_g}{\partial \eta} \delta N_e. \tag{40}$$

Where E_g is the energy bandgap and δN_e is the number of electrons or holes. Moreover for simply conservation of energy, each generated phonon will absorb (E-Eg) energy to the phonon energy E. Then the contribution to the stress is given by:

$$\sigma = -\frac{3B\beta}{C}(E - E_g)\delta N_e. \tag{41}$$

In fact this interesting result provides the possibility to detect changes in stress as a function of hot carriers, moreover in chapter 3 we proved that changes in carriers produces changes in refraction index, which are proportional to changes in reflectance, therein the reason to be able to detect such changes in stress due to phonons with our experimental setup.

4.4 Phonons generation and detection

As we showed in chapter 3, relaxation and recombination time constants are defined in a picoseconds range, this means that phonons period should be smaller than recombination and relaxation time constants because

phonons generation occurs in the cooling processes which has as a main objective to achieve an equilibrium state of the carriers in the semiconductor.

Now regarding to the experimental part, we know that phonons are generated as a consequence of momentum conservation; this means that we should repeat the experiment done in chapter 3, but on the other hand the plot in chapter 3 does not shows any vibration or some signal that can be associated with phonons.

According to the explanation of heat pulses and stress pulses, which were pointed out before, we should change the temperature or to find the way to improve phonons generation in order to be able to detect such stress changes. In fact the first idea is quite interesting and as we will show it later, temperature dependence is important and it will allow observing different phenomena, but unfortunately such equipment is not easy to handle and the time was not enough to learn how to use it, in fact that is one of the proposal that we do in chapter 5.

It is important to mention that the detection of phonons in room temperature is not an easy task, therein the reason to use in this case the thermal advantages of metals, such as thermal expansion, which improves the phonon generation, in this thesis we used aluminum. In fact we use the next section to describe how the temperature evolve in time and how thermal properties of aluminum play the role of temperature decay constant, such conclusion allows to understand the reason to use an aluminum layer as a transducer.

Moreover we explain the influence of thermal expansion in phonons generation [53], this following the idea of Wolfe [54], making use of Stefan-Boltzmann law which can be written as follow:

$$\frac{P}{A} = \sigma_{Al/Si} T^4. \tag{42}$$

Where $\frac{P}{A}$ is the radiated power per unit of area for a Planckian emitter at temperature T, where σ is the Stefan constant, which in case to consider phonons emitted from Al to Si, the constant is given by:

$$\sigma_{Al/Si} = \frac{\pi^5 k_B^4}{15h^3}\left(\frac{e_l}{c_l^2} + \frac{e_{ft}}{c_{ft}^2} + \frac{e_{st}}{c_{st}^2}\right). \tag{43}$$

Where h is the plank constant, k_B is the Boltzmann constant, $c_{l,ft,st}$ is the phase velocity of phonons with different polarization for longitudinal, fast transversal and slow transversal modes, furthermore $e_{l,ft,st}$ are the spectral emissivities which takes into account the modes conversion in the interface as well as reflection and refraction.

Then we can rewrite the expression 42 as:

$$\frac{dE}{dt} = -\sigma_{Al/Si} A T^4. \tag{44}$$

This step is very important because we introduce characteristics of aluminum by expressing the energy as a function of the density of the material ρ, the specific heat constant α, changes in temperature ΔT and volume $\Delta \upsilon$ as well as the thermal expansion ς, which allows writing the following expression:

$$E = -\rho\alpha \frac{\Delta\upsilon}{3\varsigma\Delta T} T^4 / 4. \quad (45)$$

Which can be substituted in equation (44), where $\wp = \frac{12\varsigma\Delta T}{\rho\alpha\Delta\upsilon}\sigma_{Al/Si}$ is the decay rate, which is proportional to the thermal expansion.

$$\frac{dT^4}{dt} = -T^4 / \wp. \quad (46)$$

Then this part shows a heat pulse evolving in time, in fact this demonstrate the convenience to add a metal layer called transducer. Therein the reason to add 30 nm of aluminum layer next to the silicon layer.

4.5 Experimental results.

In chapter 3 we have the pump probe experiments of this sample without the Al layer and its results are a convenient reference for our experimental results of this section where we show reflectance measurement and transmittances to corroborate our results.

After the Al layer was added to our sample, we used the experimental setup showed in figure (12B) of chapter 3. In order to detect the propagated phonons, we focus the pump beam on the aluminum layer and the probe beams on the silicon layer. It is important to mention that we did the same experiment at different wavelengths. However, we did not obtain any information related with phonons but at 800 nm we saw interesting changes on our reflectance measurements as shown in figures 24, 25 and 26 taken with different wavelengths.

Those Figures show pump probe signal without any clear phonons signal, but it shows an interesting difference compared with the pump probe signal showed in figure 16 and figure 19 of chapter 3. The main difference is in the step without and with the Al layer. The positive step in the pump probe signal correspond to the case with an Al layer, while the negative step, obtained before in chapter 3, corresponds to without.

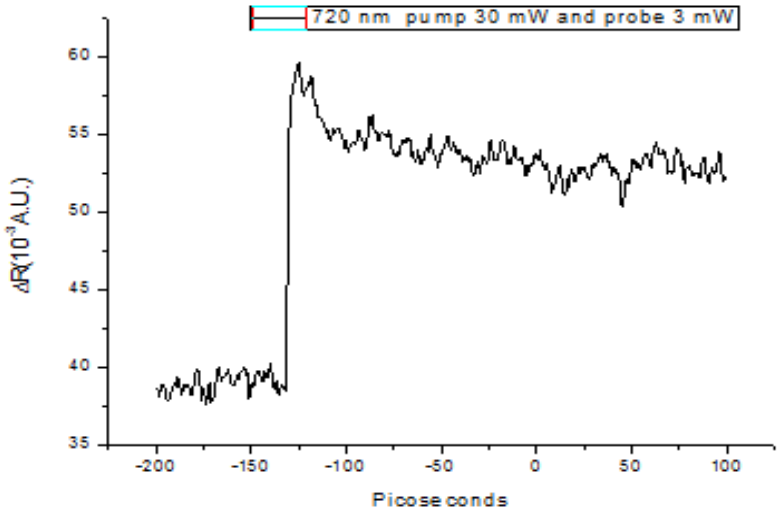

Fig. 24. Pump probe reflectance measurements, in SiOG with aluminum layer using a wavelength of 720 nm.

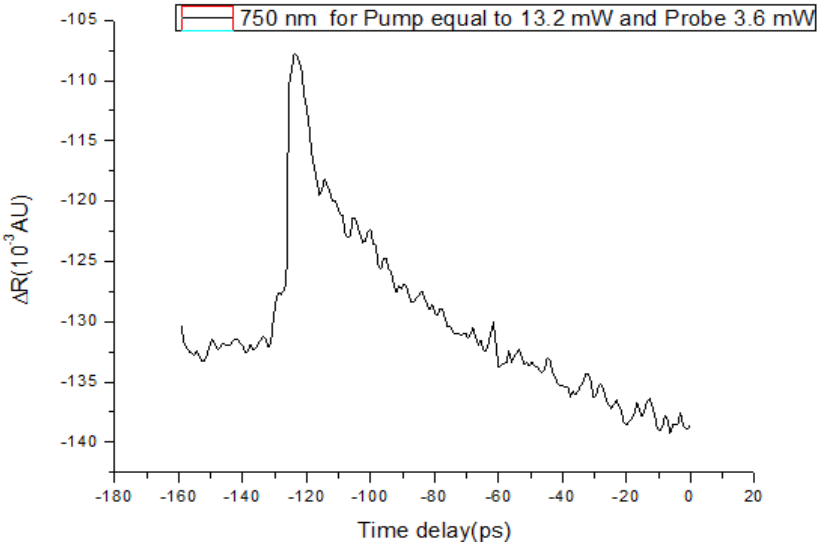

Fig 25. Pump probe reflectance measurements, in SiOG with aluminum layer using a wavelength of 750 nm.

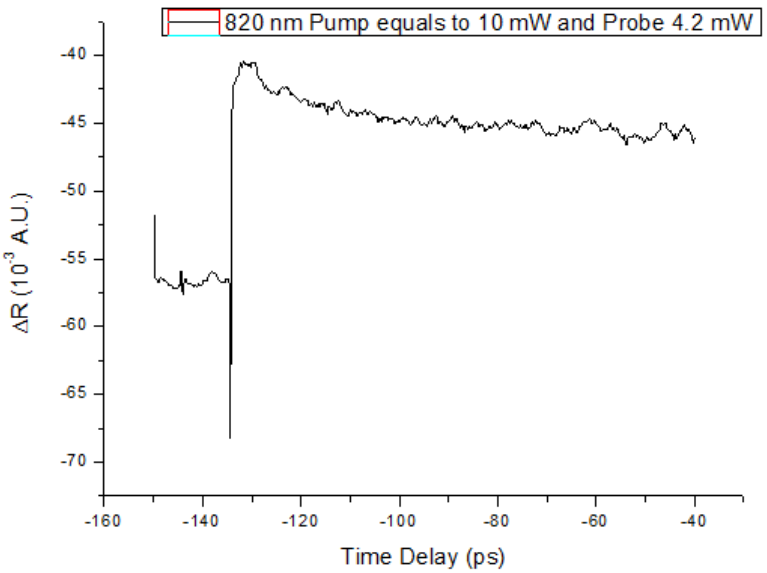

Fig 26. Pump probe reflectance measurements, in SiOG with aluminum layer using a wavelength of 820 nm.

Then using the ideas proposed by Professor Sobolewski and Professor Fauchet et al [55], in relation to the role of the real and imaginary parts of refraction index defining the pump probe step, to explain the changes in the step reflectance. We can determine, in a simple way, the reasons for those changes in ΔR after the aluminum layer was added. It is convenient to obtain the behavior of the real and imaginary parts of refraction index for aluminum, $n_{\mathrm{Re}}(\lambda)$ and $n_{im}(\lambda)$ respectively. We show such behaviors in the following figure:

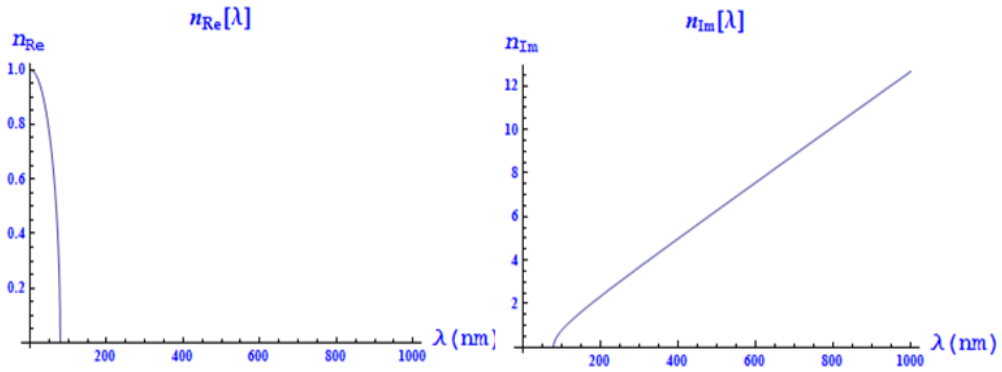

Fig 27. Real and imaginary part of refraction index as a function of the wavelength for aluminum.

They tell us that for a metal like the aluminum, we can attribute those changes in the reflectance to the basic properties of the imaginary part of refraction index and neglect the dispersion behavior given by the real part. Figure 27 will tell us how strong the metal will absorb the light. We can obtain the reflectance or transmittance, which varies with the aluminum thickness and frequency, as shown in figure 28:

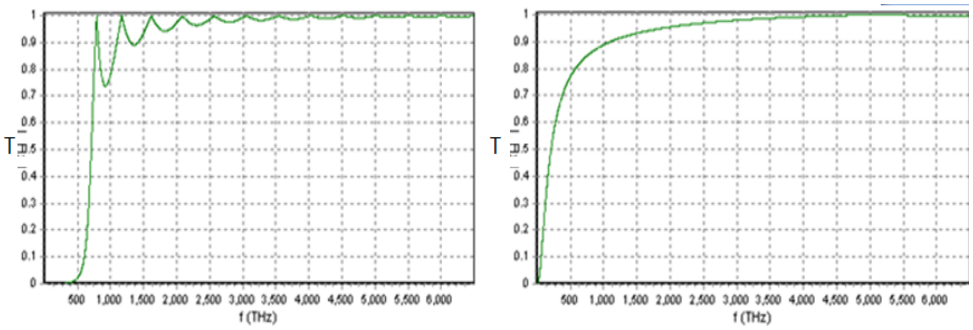

Fig 28. Transmittance depending on frequency in aluminum with a thickness of 300 nm (left) and 30 nm (right).

They demonstrate the effect observed in the sample with 30 nm aluminum layer for the wavelengths that we used. However at 800 nm, we observed some remarkable results as shown in the following figures.

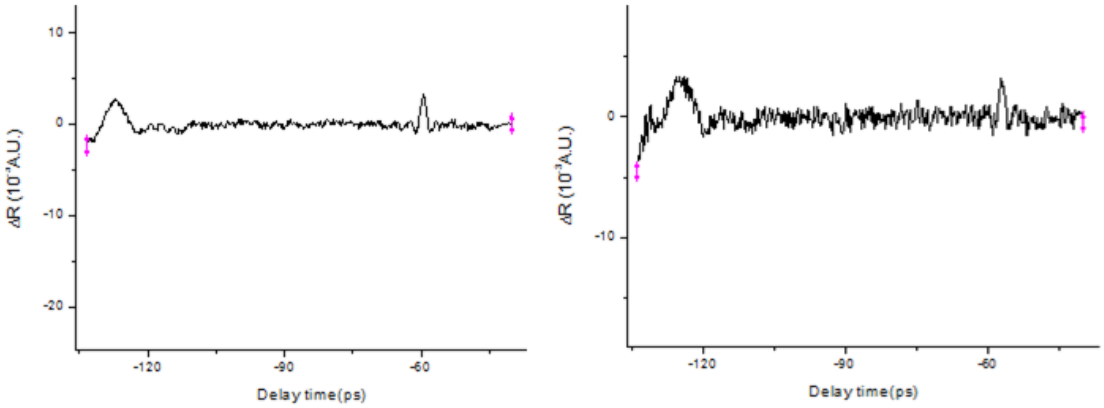

Fig 29. Pump probe reflectance measurements, in SiOG with aluminum layer using a wavelength of 800 nm.

It is important to mention that all of them are similar in shape. The plots showed before are a mixture of three phenomena: aluminum pump probe response, carrier dynamics influence and phonons dynamics. In addition of this mixture, there are two clear peaks, which are the phonons response. In order to isolate them, we subtract the pump probe signal from the curve produced by carrier dynamics, and obtain the following plots:

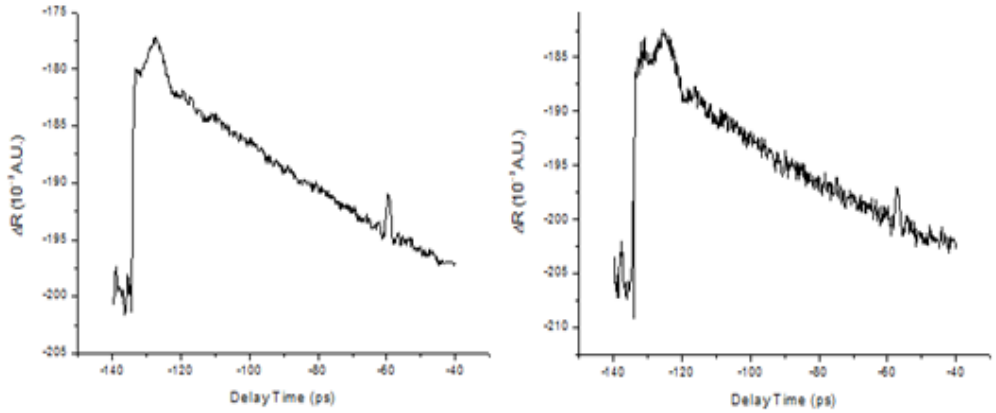

Fig 30. Pump probe reflectance signals without background signal.

In fact, such signals are not the typical signals with a clear interference pattern due to different phonons wave fronts; see [56] and [57].

One interesting result is the average distance between the two peaks, which is 67.76 ps, with a minimal standard deviation. Under the same dispersion of data, the amplitude of the first and second peak are 4.21 and 3.25 respectively, and moreover the width of the first peak as 9.7 ps and the second is 3.3 ps.

In order to corroborate these experimental results, we carried on transmittance measurements using the corresponding setup to the

reflectance configuration as shown in figure 12 C of chapter 3. After the experiment was done, we obtain the following behavior:

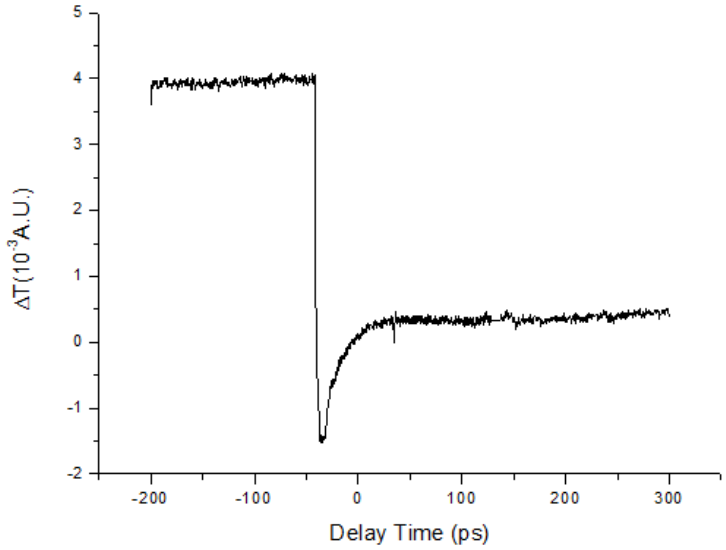

Fig 31. Pump probe transmittance measurements, in SiOG with aluminum layer using a wavelength of 800 nm.

It is important to mention that this kind of plots are just useful to verify the previews behavior, and as can be seen from the figure above, because the transmitted light is very small and is hard to obtain a better pump probe signal, and still harder to obtain details of the phonons oscillations. Therefore our theoretical analysis takes as experimental data the reflectance plots.

The behavior shown in the reflectance plot is confirmed by the transmittance plot taken with the same wavelength, which has the second peak at almost the same distance than in the previews plot.

4.6 Theoretical model of coherent acoustic phonons

Our typical-metal semiconductor structure to create phonons shows an interesting complex dynamics. The Al nano-layer plays an interesting role as a transductor not only by allowing the transmission of light by its thickness,

but in particular by transforming the light pulse into a phonon packet and by generating the phonons in a thermal process of the light absorption by the metal. Those two separate processes may be pictorially described in the following figure.

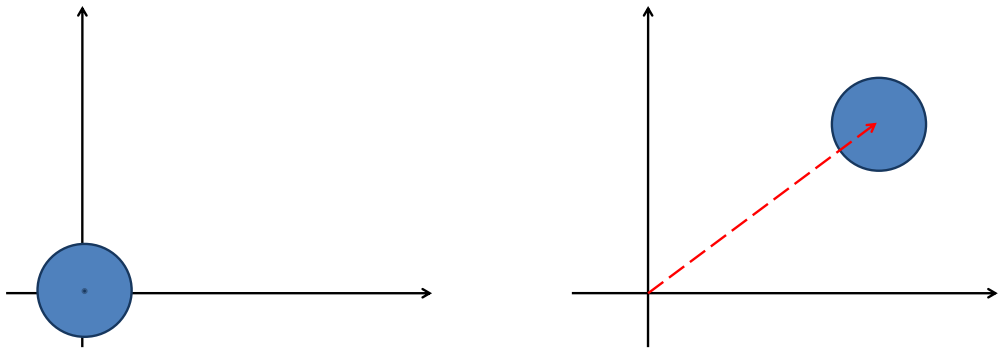

a b

Fig 32.- The figure on the left shows the initial phonons distribution without a coherent signal, and the right figure shows the phonons over the coherent pulse.

At the metal semiconductor interface occurs the thermal phonon generation, Fig. 32a, that will superimpose on the transduced phonon signal that propagates as a phonon.

The initial phonon thermal distribution P_{Th} may be described as in fig (36) as a distribution of the wave number k, and could be well described by a Planck source. The metal role as a transductor is to allow the thermal phonon distribution to ride on the transduced coherent signal pulse. This could be understood in the traditional mixed thermal coherent distribution, where;

$$P_{ThC} = P_{Th} \otimes P_C . \tag{47}$$

There, the delta like coherent distribution P_C shifts the thermal distribution but preserving its basic thermal properties. This thermal phonons riding on the transduced coherent signal could be described as a propagating wavepacket:

$$\psi(x,t) = \int_{-k_0-\Delta k}^{k_0+\Delta k} N(k) e^{-i(\omega t - kx)} dk. \tag{48}$$

Where $N(k)$ the thermal phonons density as a function of k_0 is the phonon carrier wave number and Δk the wave number range, that we will demonstrate, corresponds to a finite Δk as a Quantum Mechanical consequence at appendix A. If the dispersion relation were that of a regular classical wave $\omega \equiv kc$ this problem will become straightforward. However, a quantum mechanical description of the phonons, where the energy is given by $E = \hbar\omega$ and $E = \frac{\hbar^2 k^2}{2m}$, results in a quadratic dispersion relation $\omega = \frac{\hbar}{2m} k^2$ whose wavepacket propagation description is not an easy task. [50]. In appendix B we discussed the behavior of our wavepacket for a an infinitum k domain. We show there the expect decay behavior

Once we have defined our action plan, our first task is to determine the thermal phonon density $N(k)$. By using the adiabatic approximation proposed by Oppenheimer [58], we may consider the material as a structure formed only by atoms and neglecting the influence of electrons or ions. Moreover in our theoretical model we consider that the wavelength of phonons is very large compared with the lattice constant, and the microscopic limit formalism can be avoided.

This fact allows avoiding the formal use of the lattice and considering a model similar to a linear chain. The rapid rise in heat flux, which was described before, indicates that a significant number of subterahertz phonons are quickly produced by the decay of several-terahertz phonons. Thus, we are dealing with a broad and changing distribution of frequencies. Therefore, we may consider the detected phonons as a diffusive motion of phonons, described by the kinetic equation [59], [60]:

$$\left(\frac{\partial}{\partial t} - D\nabla^2\right) N(r,t) = N_0 \delta(r)\delta(t). \tag{49}$$

Where D is the diffusion constant that describes how fast the phonons diffuse. $N(r,t)$ is the number of thermal phonons density at time t, position r, and $N_0\delta(r)\delta(t)$ are the generated phonons in the aluminum film as initial conditions for the wavepacket. After the kinetic equation was solved in spherical coordinates, with no approximations due to the small dimensions of the Al layer, the following solution was found:

$$N(r,\tau) = N_0 (4\pi D\tau)^{-\frac{3}{2}} e^{-\frac{r^2}{4D\tau}} = \Omega e^{-\frac{r^2}{2\sigma^2}}. \tag{50}$$

This expression can be understood as the initial phonon distribution and recognize it as a gaussian distribution on the radius position and width $\sigma^2 = 2D\tau$.

In order to describe the wave packet propagation given in Eq. 51 we will consider only the longitudinal acoustic phonons to obtain the phonon density $N(k)$ as function of k .

$$N(k,\tau)=\frac{1}{\sqrt{2\pi}}\int_{-\infty}^{\infty}N(r,\tau)e^{-ikr}dr=\sigma\sqrt{2\pi}e^{-\frac{\sigma^2k^2}{2}}. \tag{51}$$

Then the expression (49) gives the initial distribution at the time τ in the spatial frequency domain, that may be considered as the initial phonon distribution to be driven by the pulse and given by:

$$\psi(x,t)=\int_{-k_0-\Delta k}^{k_0+\Delta k}N(k)e^{-i(\omega t-kx)}dk. \tag{52}$$

Where the time evolution is governed by the Quantum Mechanical character of the phonons i.e.

$$\omega=\frac{\hbar}{2m}k^2. \tag{53}$$

In order to explore this solution, let us define the associated wavepacket function

$$\psi(x_0,t;k)=\int_{-k}^{k}N(k')e^{-i(\omega' t-k' x_0)}dk'. \tag{54}$$

for a fixed x_0 and described pictorically in Figure 33, as a function of time *t*, Fig. 33a, and as a function of *k*, Fig. 33b. We can notice a clear resemblance of the short time behavior, Fig 33a, and the experimentally observed data.

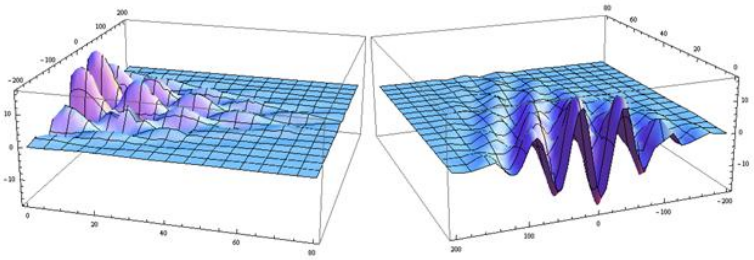

a b

Fig 33. Time dependence (a) and the *k* dependence (b) for a fixed x_0 of equation 52

However Fig, 33b shows us that this function is quite complicated, this can be seen in the following solution.

$$\psi(x,t)=\int_{k_0-\Delta k}^{k_0+\Delta k} N(k')e^{i(k'x-\frac{\hbar k'^2}{2m}t)}dk'=\int_{k_0-\Delta k}^{k_0+\Delta k} e^{\Delta x k'^2}e^{i(k'x-\frac{\hbar k'^2}{2m}t)}dk'$$

$$=\frac{(1+i)e^{-\frac{mx^2}{2i\hbar t-4m\Delta x}}\sqrt{\frac{m\pi}{2}}}{2\hbar^2t^2+8m^2\Delta x^2}\left(\begin{array}{l} e^{i\frac{\hbar mtx^2}{\hbar^2t^2+4m^2\Delta x^2}}\left(-i\hbar t+2m\Delta x\right)\sqrt{i\hbar t+2m\Delta x}\left(\begin{array}{l} Erf\left(\frac{i\hbar(k_0+\Delta k)t+imx+2(k_0+\Delta k)m\Delta x}{\sqrt{2m(i\hbar t+2m\Delta x)}}\right)\\ -Erf\left(\frac{i\hbar(k_0-\Delta k)t+imx+2(k_0-\Delta k)m\Delta x}{\sqrt{2m(i\hbar t+2m\Delta x)}}\right)\end{array}\right)\\ +\left(-i\hbar t-2m\Delta x\right)\sqrt{-i\hbar t+2m\Delta x}\left(\begin{array}{l} Erfi\left(\frac{\hbar(k_0+\Delta k)t+m\left(x+2i(k_0+\Delta k)\Delta x\right)}{\sqrt{2m(-i\hbar t+2m\Delta x)}}\right)\\ -Erfi\left(\frac{\hbar(k_0-\Delta k)t+m\left(x+2i(k_0-\Delta k)\Delta x\right)}{\sqrt{2m(-i\hbar t+2m\Delta x)}}\right)\end{array}\right)\end{array}\right). \quad (55)$$

Moreover it is important to be aware about the role that plays the Gaussian width. When the Gaussian is narrower or $(\Delta x)^{-1}$ is smaller than k the recurrence effect that we will defined later will not be possible, then in the opposite situation when k is smaller than $(\Delta x)^{-1}$, or in other words a wider Gaussian, this will allows to have the recurrence effect.

Therefore we will consider some approximations to grasp the idea of what sort of solutions we have ahead. Let assume that the range Δk is small enough to consider $N(k')$ a constant Υ in that region of the spatial frequency domain, then we obtain:

This simplified method derives an expression of complex functions. However, the important point is to realize that in addition of the short time behavior, there is an interference between the espectral limits $\pm\Delta k$ that will show at longer times when the phases matches. Let us assume that Δk is

smaller than k_0. Let us consider the small time limit, when de phonon dispersion sets up, and we obtain, see appendix C:

$$\psi(x,t)=\int_{-\Delta k}^{\Delta k}\Upsilon e^{ikx-i\frac{\hbar t}{2m}(k_0+\delta k)^2}d\delta k\simeq 2\Upsilon e^{-i(\omega_0 t-k_0 x)}Sinc\left[\Delta k(\frac{hk_0}{m}t+x)\right]. \tag{56}$$

Where $\omega_0=\frac{\hbar k_0^2}{2m}$ and $v_o=\frac{hk_0}{m}$.

In fact, this shape looks quite similar to the one obtained in the experiment, and surely this should be the responsible for the first peak. But this explanation is not complete because it does not provide any information related with the second peak, but it provides information about the nature of the peaks, which is a kind of sinc function. After a given time T, and because the finite spectral limit, our wavepacket can suffers a phase matching:

$$\Delta\phi=\hbar\frac{\left(k_0+\Delta k\right)^2-\left(k_0-\Delta k\right)^2}{2m}T=2\pi=\hbar\frac{2k_0\ \Delta k}{m}T. \tag{57}$$

Where:

$$T_r=\pi\frac{m}{\hbar\ k_0\Delta k}.$$

Lets us point out, that we have applied phase matching conditions to the solution of a Schroedinger Equation and not to an Electromagnetic one, therefore to this reconstruction of the signal we will call recurrence, to distinguish from the revivals due to the QED nature of the QED field-matter interaction.

If we substitute t by T_r+ τ in the wavepacket expression, where τ is the local time, and as can be seen in appendix D, χ is the local position, this allows obtaining:

$$\psi(x,t)=\int_{-\Delta k}^{\Delta k}\Upsilon e^{ikx-i\frac{\hbar(T+\tau)}{2m}(k_0+\delta k)^2}d\delta k$$

$$=\left(\begin{array}{l}4\sin c\left(\Delta k\frac{1}{2}\left(x_0-\frac{\hbar k_0T_r}{m}+\chi-\frac{\hbar k_0\tau}{m}-\frac{\pi}{2k_0}\right)\right)e^{-i\frac{1}{2}\Delta k\left(x_0-\frac{\hbar k_0T_r}{m}+\chi-\frac{\hbar k_0\tau}{m}-\frac{\pi}{2k_0}\right)}\\+4\sin c\left(\Delta k\frac{1}{2}\left(x_0-\frac{\hbar k_0T_r}{m}+\chi-\frac{\hbar k_0\tau}{m}+\frac{\pi}{2k_0}\right)\right)e^{-i\frac{1}{2}\Delta k\left(x_0-\frac{\hbar k_0T_r}{m}+\chi-\frac{\hbar k_0\tau}{m}+\frac{\pi}{2k_0}\right)}\end{array}\right)e^{-i\frac{\hbar(T_r+\tau)}{2m}k_0^2}e^{ik_0x}.$$

(58)

We realize that this set of slightly mismatched sinc functions correspond to a renewal of the signal, slightly different from the original one but by the mismatch $\pi/2k_0$. The bracket on T_r corresponds to the phase matching position and it is null in practice.

In spite of being this a convenient approximation, we may compare these results with those of our experiment. We know from the previews equation that T_r is the separation time between the two peaks, m is the effective mass of silicon, Δk can be calculated after fitting the experimental data, therefore we can determine the central spatial frequency k_0. Therefore after doing the fitting, using two functions similar to 52, we obtained that the best fit is given by:

$$\left(3.402*\mathrm{Sinc}\left[\frac{\pi}{4.5}*(t+131.8)\right]+3.12*\mathrm{Sinc}\left[\frac{\pi}{1.2}*(t+65)\right]\right)$$

(59)

In fact the fit is quite good, as can be seen in figure 34; this verifies our theoretical description, and the proposed idea of a finite spectrum.

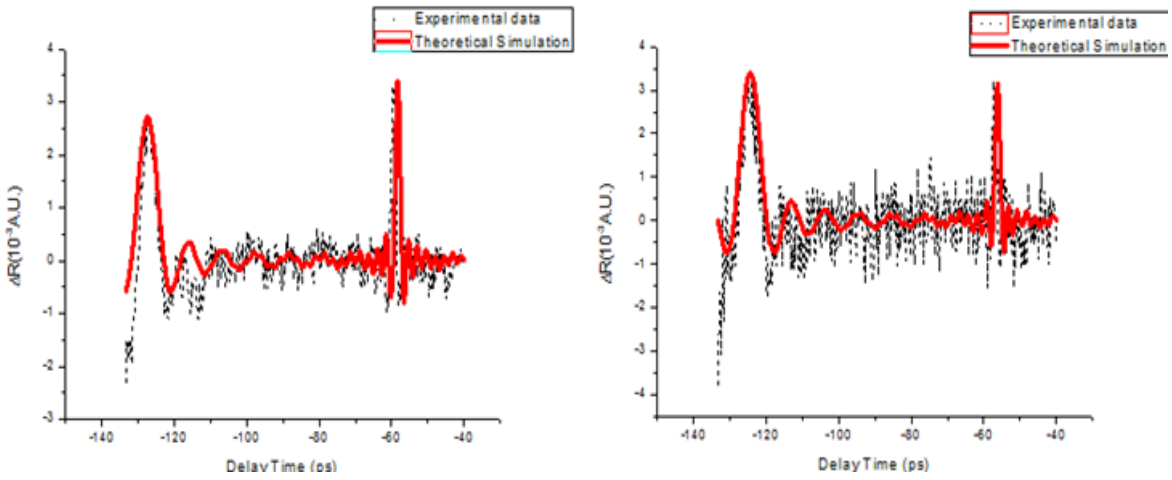

Fig 34.- Comparison of the experimental results and our Simulations, using our description as a wave packet. The description fits quite well the experimental results.

Furthermore the coherence length can be calculated, after the central spatial frequency is calculated using Eq. 58, as follow:

$$\Delta\phi = 2\Delta k \times l_c = 2\pi. \tag{60}$$

Finally using the expressions (C4) and (D2), showed in the appendix C and D, we calculated the phonons velocity as v=8002.14 m/s. This is slightly different from the 8430 m/s already reported. This is due to the dispersion produced by the temperature; in fact a ballistic phonon velocity should converge to the sound velocity, but our case is quite different and the velocity that we calculated is smaller than the reported, this is the result that we expected. Moreover we calculated the traveled distance as 536.14 nm and a frequency of 1.49 x10^{-2} THz.

It is important to point out that these results have been obtained using a quantum mechanical description; however the results shown are quite similar to those obtained from a classical description.

Chapter 5

Conclusions

5.1 Abstract

In this chapter we put together the general conclusions of the previews chapters, and allow us to propose new ideas to continue our carriers and phonons dynamics research in a near future highlighting the obtained key points.

Finally we made a proposal to fabricate photonic crystals with our sample, in fact we show some simulations that suggest that our idea can be possible.

5.2 New trends related with carrier dynamics studies

We studied and demonstrated the importance of ultrafast characterization, in particular pump probe spectroscopy. In this research we developed a theoretical model to characterize our samples by its relaxation and recombination time constants, which resulted quite useful to our needs. In fact we formulated an expression that allows knowing more fundamental data related with carriers and its probability function as well as refraction index.

In chapter 3 we related changes in refraction index with the hot carriers concentration. A deeper and interesting study is the real and imaginary parts of the dielectric permittivity, and the behavior of susceptibilities, during the recombination and relaxation processes. In fact, the nature of the pump probe experiment allows us studing nonlinear effects due to the intensity of the

pump light. Then the study of nonlinear effects in silicon becomes a possibility, as well as the study of the intrinsic properties of silicon, such as permittivity and susceptibilities, and moreover the time and functional form of the nonlinear terms can be described.

Other important parameter that we have mentioned but not studied in this thesis, when the energy band gap was calculated, is the absorption function of the silicon on glass with a barrier layer. The silicon on glass absorption has been widely reported; however, the role of the barrier layer in the absortion is not known yet and becomes quite important when a device will be designed. Furthermore such absorption function is related with the occupancy functions of carriers in the semiconductor.

Finally, a temperature map of the material can be obtained by solving the following coupled system:

$$\begin{aligned} C_{Carriers}\frac{\partial T_{Carriers}}{\partial t} &= K\nabla^2 T_{carriers} - \alpha(T_{carriers} - T_{lattice}) + A(r,t) \\ C_{lattice}\frac{\partial T_{lattice}}{\partial t} &= \alpha(T_{carriers} - T_{lattice}). \end{aligned} \tag{61}$$

Where $C_{Carriers}$ and $C_{lattice}$ are the heat capacities of carriers and lattice respectively, $T_{Carriers}$ and $T_{lattice}$ are the temperature of carriers and lattice, then α is the electron-phonon coupling, K is the thermal conductivity and $A(r,t)$ is the incident optical pulse, in our case is $A(r,t) = I_0(r,t)e^{-4\ln 2\frac{t^2}{\tau_p{}^2}}$.

The previous system allows building an image of the heat pulse propagating in space and time, which is a proposal to do phonon imaging.

In fact the previous equations are not an easy system to solve. It is important to realize that the electron-phonon coupling is a function of time. Under the treatment we have developed, the behavior also depends on the k-space. All those factors become the previous equation in a complicated nonlinear equation, which is part of the future work that we plan to pursue.

5.3 New trends related with phonos dynamics studies and posible engineering of our SIOG sampple

One of the most important results in this thesis is to provide a description on the transducer function, and the coherent characteristic that it is attributed to the generated thermal phonons. Moreover we demonstrate that we generated a finite frequency range of phonons and the reason to have such finite spectrum is related with the quantum behavior of phonons and temperature conditions.

The last comment is related with future studies of phonons dynamics, we are interested on being able to distinguish the phonons purely thermal behavior: This is done by isolating the coherent characteristic attributed by the transducer, and to provide a detailed explanation of that behavior. Moreover it wll be interesting to develop a study of the coherent characteristics of the phonons. This will allow us to make important predictions in this interesting field.

Finally in collaboration with Adalberto Molina, a group member, we started to develop an analysis of our sample in order to make a proposal to develop a photonic crystal; in fact this seems to be possible after we realized some simulations, and this can be seen in the following figure.

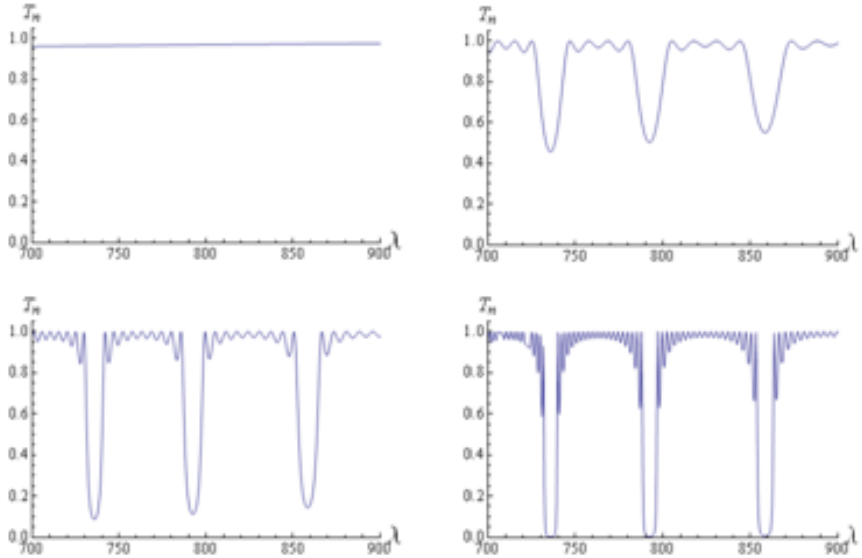

Fig 35. Transmittance measurements, after use our sample, as a photonic crystal.

The upper figure on the left was obtained using just one period of the sample, the seconds is with 5 periods, the third with 10 periods and the fourth with 20 periods.

The figure above shows the photonic bands, which tell us that the fabrication of the photonic crystal is possible using our sample.

Apendix A.

One of the most striking experimental observations is the identification of the behavior of the wavepacket as a defasing and recurrence behavior, and therefore our proposal of finite wave number spectra. This is a peculiar proposal of a cut-off frequency ω_c which needs to be elaborated on. Therefore we include a common analisis found in the literature for the thermal dispersion in a Planck source as the description of the thermal phonosn, before being displaced by the coherent signal, Fig. 32a.

Let us consider the energy of Plank oscillators as a random variable defined by $E_n(\omega)=\left(n+1/2\right)\hbar\omega$ and probability given by $p_n=\frac{1}{\Gamma}e^{-\frac{E_n}{k_BT}}$ where Γ is a normalized factor. Moreover $E_1<E_2<...<E_n$ and $\tilde{E}$ is the average energy, which has to satisfy:

$$\tilde{E}(\omega)=\frac{\hbar\omega}{e^{\frac{\hbar\omega}{k_BT}}-1}>E_0. \qquad \text{(a1)}$$

In the following figure, we illustrate $E_0(\omega),E_1(\omega),E_2(\omega)...$ and $E_n(\omega)$ as a function of frequency.

In fact from such figure, one can define the cut-off frequency ω_c just by finding out the point where the Gaussian (black line) or Planckian (blue line) distribution intersects the energy function for the Planck oscillators $E=\hbar\omega$.

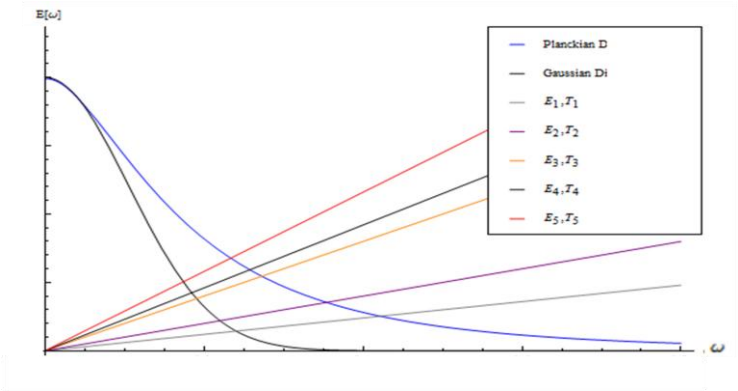

Fig. A1 The intersection of Planck oscillators with the Gaussian and Planck distribution defines the cut-off frecuency.

From figure 1, it is clear that for each frequency $\omega > \omega_c$ the expression a1 is not valid, then for a certain temperature T the oscillators with the frequency $\omega > \omega_c$ cannot be excited. This fact defines the cut-off frequency which can be calculated by:

$$\frac{\hbar\omega_c}{e^{\frac{\hbar\omega_c}{k_B T}} - 1} = \hbar\omega_c. \tag{a2}$$

Where

$$\omega_c = \frac{k_B T}{\hbar} \ln 2. \tag{a3}$$

The preview equation shows the dependence of the cut-off frequency with the temperature. This fact cuts one part of the entire spectrum and agrees with our expectations for the spread out of a ballistic signal at low temperature, where the spread out should be the quantum minimum energy of $E_0(\omega) = \frac{1}{2}\hbar\omega$.

Now if we think in our experiment, it has been specified that the experiment was done in a room temperature after the Al transducer that shifts the origin

to k_0. This fact produces the finite spectrum in the k-space described in Fig. 32b. The definition of the limiting wavevectors would be given by,

$$\left|k_0 \pm \Delta k\right| = \frac{\omega_{\pm}}{c}\sqrt{\varepsilon\mu}. \tag{a4}$$

Appendix B.

A Gaussian of a given width Δx, with ±∞ limits , may be a reasonable assumption for a limited thermal-coherent phonon k distribution in exchange for sharp limited distribution discussed in Eq.d3 in appendix D. This problem has been discussed long ago for wavepackets by L. Schiff in his text of Quantum Mechanics. There he discused the time evolution of a gaussian wavepacket, centered at the origen, decribed in the equation a1.

$$\psi = \left[\frac{(\Delta x)^2}{2\pi^3}\right]^{\frac{1}{4}} \int_{-\infty}^{\infty} e^{\left[-k^2(\Delta x)^2 - \frac{i\hbar k^2 t}{2m} + ikx\right]} dk = (2\pi)^{-\frac{1}{4}} \left(\Delta x + \frac{i\hbar t}{2m\Delta x}\right)^{-\frac{1}{2}} e^{-\frac{x^2}{4(\Delta x)^2 + \left(\frac{2i\hbar t}{m}\right)}}. \tag{b1}$$

Whose squared modulus is given by:

$$|\psi|^2 = \left\{2\pi(\Delta x)^2\left[1 + \frac{\hbar^2 t^2}{4m^2(\Delta x)^4}\right]\right\}^{-\frac{1}{2}} e^{-\frac{x^2}{2\left[(\Delta x)^2 + \frac{\hbar^2 t^2}{4m^2(\Delta x)^2}\right]}}. \tag{b2}$$

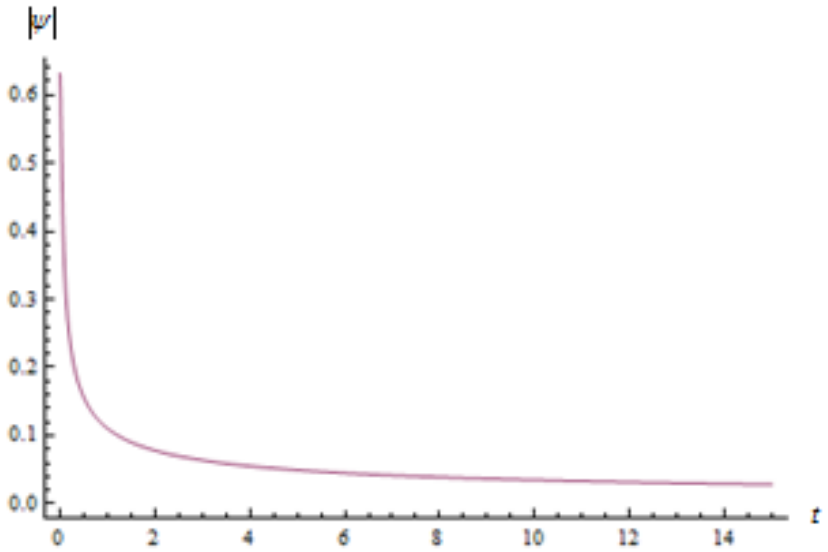

Fig.B1. Module of Psi function evolving with the parameter t.

That can be rewritten as in the figure above:

$$|\psi|^2 = \left\{ 2\pi (\Delta x)^2 \left[1 + \frac{t^2}{T_0^2} \right] \right\}^{-\frac{1}{2}} e^{-\frac{x^2}{2(\Delta x)^2 \left[1 + \frac{t^2}{T_0^2} \right]}}. \tag{b3}$$

Where the careacteristic decay time is given by:

$$T_0 = (\Delta x)^2 \, 2m/\hbar. \tag{b4}$$

A crude approximation for the short time behavior demonstrates the expected short time decay:

$$|\psi|^2 == \left[\left\{ 2\pi (\Delta x)^2 \right\}^{-\frac{1}{2}} e^{-\frac{x^2}{2(\Delta x)^2}} \right] e^{-\frac{t^2}{2T_0^2}}. \tag{b5}$$

However, a longer time behavior is better describer by a gaussian decay produced for an increasing with $\sigma(t) = (\Delta x) \left[1 + \frac{t^2}{T_0^2} \right]^{-\frac{1}{2}}$.

(b6)

The role of the transducer is to introduce a coherent signal, that corresponds to a shift to the Gaussian by k_0 in the Schiff integral.

$$\psi = \left[\frac{(\Delta x)^2}{2\pi^3} \right]^{\frac{1}{4}} \int_{-\infty}^{\infty} e^{\left[-(\kappa - k_0)^2 (\Delta x)^2 - \frac{i\hbar\kappa^2 t}{2m} + i\kappa x \right]} d\kappa. \tag{b7}$$

If we introduce the change of variables $\kappa = k + k_0$ and $x = x - vt$, where $v = \hbar k/m$, we finally obtain :

$$\psi=\left[\frac{(\Delta x)^2}{2\pi^3}\right]^{\frac{1}{4}}\int_{-\infty}^{\infty}e^{\left[-k^2\Delta x^2-i\frac{h}{2m}(k-k_0)^2t+i(k+k_0)x\right]}dk=\left[\frac{(\Delta x)^2}{2\pi^3}\right]^{\frac{1}{4}}e^{i\frac{h}{2m}k_0{}^2t+ik_0x}\int_{-\infty}^{\infty}e^{\left[-k^2\Delta x^2-i\frac{h}{2m}k^2t+ikx-i\frac{h}{2m}2kk_0t\right]}dk$$

$$=\left[\frac{(\Delta x)^2}{2\pi^3}\right]^{\frac{1}{4}}e^{i\frac{h}{2m}k_0{}^2t+ik_0x}\int_{-\infty}^{\infty}e^{\left[-k^2\Delta x^2-i\frac{h}{2m}k^2t+i\left(x-\frac{h}{m}k_0t\right)k\right]}dk=\left[\frac{(\Delta x)^2}{2\pi^3}\right]^{\frac{1}{4}}e^{i\frac{h}{2m}k_0{}^2t+ik_0x}\int_{-\infty}^{\infty}e^{\left[-k^2\Delta x^2-i\frac{h}{2m}k^2t+i(x-vt)k\right]}dk.$$

(b8)

Where we can finally can recognize the Schiff integral and therefore the final expression:

$$\psi=\left[\frac{(\Delta x)^2}{2\pi^3}\right]^{\frac{1}{4}}e^{i\frac{h}{2m}k_0{}^2t+ik_0x}\int_{-\infty}^{\infty}e^{\left[-k^2\Delta x^2-i\frac{h}{2m}k^2t+iXk\right]}dk=(2\pi)^{-\frac{1}{4}}\left(\Delta x+\frac{i\hbar t}{2m\Delta x}\right)^{-\frac{1}{2}}e^{i\frac{hk_0{}^2t}{2m}+ik_0x}e^{-\frac{(x-vt)^2}{4(\Delta x)^2+\left(\frac{2i\hbar t}{m}\right)}}.$$

(b9)

The modulus of $|\psi|$ removes the fase factors and we obtain a similar expression to that without a coherent signal.

$$|\psi|^2=\left\{2\pi\left[(\Delta x)^2+\frac{\hbar^2t^2}{4m^2(\Delta x)^2}\right]\right\}^{-\frac{1}{2}}e^{-\frac{(x-vt)^2}{2\left[(\Delta x)^2+\frac{\hbar^2t^2}{4m^2(\Delta x)^2}\right]}}=\left\{2\pi(\Delta x)^2\left[1+\frac{t^2}{T_0^2}\right]\right\}^{-\frac{1}{2}}e^{-\frac{(x-vt)^2}{2(\Delta x)^2\left[1+\frac{t^2}{T_0^2}\right]}}.$$

(b10)

It is quite evident from this expression, that the introduction of a coherent signal, will not introduce any modification of the decay but a propagation effect. Let us notice, that eventhough that we have introduced k_0, we have not find out how to measure it.Finally, let us compare this decay time with our recurrence time observed experimentally:

$$T_0/T_r=2\pi k_0\Delta k(\Delta x)^2.$$

(b11)

We are tempted to consider that such recurrence could be due to a concentrated k-distribution rather than a sharp limited distribution. In such a case $2(\Delta k)^2(\Delta x)^2\approx 1$ and

$$T_0/T_r\approx 2\pi k_0\Delta k/2(\Delta k)^2=\pi k_0/\Delta k.$$

(b12)

Appendix C.

In this section we will compute the analytical expression for the dephasing, and in Appendix 4 the recurrence, of the wave packet of a square k distribution as an example of a sharply limited k distribution. We shall assume that $\Delta k / k_0$ is small, therefore we could assume the integration variable $\left|\delta k / k_0\right|$ is much smaller $|\delta k| \le \Delta k$.

We can define the wavepacket of a square spectrum with amplitude Υ as described by:

$$\psi(x,t) = \int_{-\Delta k}^{\Delta k} \Upsilon e^{ikx - i\frac{\hbar t}{2m}(k_0+\delta k)^2} d\delta k. \tag{c1}$$

For the dephasing of this wavepacket, we can consider δk very small and δk^2 negigible for small t. We can approximate.

$$\psi(x,t) \approx \int_{-\Delta k}^{\Delta k} \Upsilon e^{ikx} e^{-i\frac{\hbar t}{2m}({k_0}^2 + 2k_0\delta k)} d\delta k = e^{-i\frac{\hbar t}{2m}k_0^2} \int_{-\Delta k}^{\Delta k} \Upsilon e^{ikx - i(\frac{\hbar t}{m}k_0)\delta k} d\delta k. \tag{c2}$$

Moreover k is defined as $\delta k + k_0$ where k_0 is the central spatial frequency.

$$\psi(x,t) = e^{-i\frac{\hbar k_0^2}{2m}t}\Upsilon\int_{-\Delta k}^{\Delta k} e^{i(\delta k + k_0)x - i\frac{\hbar k_0}{m}t}\, d\delta k = e^{-i\frac{\hbar k_0^2 t}{2m}} e^{ik_0 x}\Upsilon\int_{-\Delta k}^{\Delta k} e^{i(\delta k)x - i\frac{\hbar k_0 t}{m}\delta k}\, d\delta k$$

$$= e^{-i\frac{\hbar k_0^2 t}{2m}} e^{ik_0 x}\Upsilon\int_{-\Delta k}^{\Delta k} e^{i\left(x - \frac{\hbar k_0 t}{m}\right)\delta k}\, d\delta k = \Upsilon e^{-i(\omega_0 t - k_0 x)} Sinc\Delta k\left(x + \frac{hk_0}{m}t\right)$$

$$= \Upsilon e^{-i(\omega_0 t - k_0 x)} Sinc\Delta k\left(\frac{hk_0}{m}t + x\right).$$

(c3)

Where the frequency and velocity is defined as follow:

$$v_o = \frac{hk_0}{m}$$

$$\omega_0 = \frac{\hbar k^2{}_0}{2m}$$

(c4)

Appendix D

The coherent evolution of the phonons, of the limited spectra wave packets, allows using native phenomena of waves such as phase matching that would occur after a given certain time. This can be obtained as follow:

$$\Delta\phi = \hbar \frac{k_1^2 - k_2^2}{2m} T = 2\pi$$
$$= \hbar \frac{(k_1 - k_2)(k_1 + k_2)}{2m} T = \hbar \frac{k_0 2\Delta k}{m} T. \quad \text{(d1)}$$

Then we can write k_0 and T as follow:

$$k_0 = \pi \frac{m}{T\hbar\Delta k}. \qquad T = \pi \frac{m}{\hbar k_0 \Delta k}. \quad \text{(d2)}$$

In this section we will compute the analytical expression for the recurrence at this time T, that cannot be considere small enough $T\Delta k = \pi \frac{m}{\hbar k_0}$. Therefore we define the local time τ and position χ, where we could assume the integration variable $\left| \delta k / k_0 \right|$ as small in terms of local variables.

Using the previous definitions we can add in the particle propagator the local time and position. Now we substitute t by T+ τ in the wavepacket expression, where τ is the local time, and x as x0 +χ, χ is the local position and x0 is the central position, under those assumptions and taking into account the previous definition we developed the following procedure:

$$\psi(x,t)=\int_{-\Delta k}^{\Delta k}\Upsilon e^{ikx-i\frac{\hbar(T+\tau)}{2m}(k_0+\delta k)^2}d\delta k\simeq\int_{-\Delta k}^{\Delta k}\Upsilon e^{ikx}e^{-i\frac{\hbar(T+\tau)}{2m}(k_0{}^2+2k_0\delta k+(\delta k)^2)}d\delta kha$$

$$=e^{-i\frac{\hbar(T+\tau)}{2m}k_0^2}\int_{-\Delta k}^{\Delta k}\Upsilon e^{ikx-i(\frac{\hbar(T+\tau)}{m}k_0)\delta k}e^{-i\frac{\hbar(T+\tau)}{2m}(\delta k)^2}d\delta k\simeq e^{-i\frac{\hbar(T+\tau)}{2m}k_0^2}\int_{-\Delta k}^{\Delta k}\Upsilon e^{ikx-i(\frac{\hbar(T+\tau)}{m}k_0)\delta k}e^{-i\pi\frac{(\delta k)^2}{2k_0\Delta k}}d\delta k$$

$$\approx e^{-i\frac{\hbar(T+\tau)}{2m}k_0^2}\int_{-\Delta k}^{\Delta k}\Upsilon e^{ikx-i(\frac{\hbar(T+\tau)}{m}k_0)\delta k}e^{-i\frac{\pi}{2k_0}|\delta k|}d\delta k\approx e^{-i\frac{\hbar(T+\tau)}{2m}k_0^2}\int_{-\Delta k}^{\Delta k}\Upsilon e^{i(x_0+\chi)(k_0+\delta k)-i(\frac{\hbar(T+\tau)}{m}k_0)\delta k}e^{-i\frac{\pi}{2k_0}sign(\delta k)\delta k}d\delta k$$

$$\approx e^{-i\frac{\hbar(T+\tau)}{2m}k_0^2}\int_{-\Delta k}^{\Delta k}\Upsilon e^{i\left(k_0x_0-\frac{\hbar k_0T}{m}\delta k+k_0\chi+x_0\delta k-\frac{\hbar k_0\tau}{m}\delta k-\frac{\pi}{2k_0}sign(\delta k)\delta k\right)}d\delta k\approx e^{-i\frac{\hbar(T+\tau)}{2m}k_0^2}e^{ik_0x}\int_{-\Delta k}^{\Delta k}\Upsilon e^{i\left(x_0-\frac{\hbar k_0T}{m}+\chi-\frac{\hbar k_0\tau}{m}-\frac{\pi}{2k_0}sign(\delta k)\right)\delta k}d\delta k$$

$$\approx e^{-i\frac{\hbar(T+\tau)}{2m}k_0^2}e^{ik_0x}\int_{-\Delta k}^{\Delta k}\Upsilon e^{i\left(\left(x_0-\frac{\hbar k_0T}{m}-\frac{\pi}{2k_0}sign(\delta k)\right)+\chi-\frac{\hbar k_0\tau}{m}\right)\delta k}d\delta k$$

$$\approx e^{-i\frac{\hbar(T+\tau)}{2m}k_0^2}e^{ik_0x}\left(\int_0^{\Delta k}\Upsilon e^{i\left(\left(x_0-\frac{\hbar k_0T}{m}-\frac{\pi}{2k_0}\right)+\chi-\frac{\hbar k_0\tau}{m}\right)\delta k}d\delta k+\int_{-\Delta k}^{0}\Upsilon e^{i\left(\left(x_0-\frac{\hbar k_0T}{m}+\frac{\pi}{2k_0}\right)+\chi-\frac{\hbar k_0\tau}{m}\right)\delta k}d\delta k\right)$$

$$\approx\left(\frac{1-e^{-i\Delta k\left(x_0-\frac{\hbar k_0T}{m}+\chi-\frac{\hbar k_0\tau}{m}-\frac{\pi}{2k_0}\right)}}{i\left(x_0-\frac{\hbar k_0T}{m}+\chi-\frac{\hbar k_0\tau}{m}-\frac{\pi}{2k_0}\right)}-\frac{1-e^{i\Delta k\left(\left(x_0-\frac{\hbar k_0T}{m}+\chi-\frac{\hbar k_0\tau}{m}+\frac{\pi}{2k_0}\right)\right)}}{i\left(x_0-\frac{\hbar k_0T}{m}+\chi-\frac{\hbar k_0\tau}{m}+\frac{\pi}{2k_0}\right)}e^{-i\frac{\hbar(T+\tau)}{2m}k_0^2}e^{ik_0x}\right)e^{-i\frac{\hbar(T+\tau)}{2m}k_0^2}e^{ik_0x}$$

$$=\left(\left[\frac{e^{i\Delta k\frac{1}{2}\left(x_0-\frac{\hbar k_0T}{m}+\chi-\frac{\hbar k_0\tau}{m}-\frac{\pi}{2k_0}\right)}-e^{-i\Delta k\frac{1}{2}\left(x_0-\frac{\hbar k_0T}{m}+\chi-\frac{\hbar k_0\tau}{m}-\frac{\pi}{2k_0}\right)}}{i\left(x_0-\frac{\hbar k_0T}{m}+\chi-\frac{\hbar k_0\tau}{m}-\frac{\pi}{2k_0}\right)}\right]e^{-i\frac{1}{2}\Delta k\left(x_0-\frac{\hbar k_0T}{m}+\chi-\frac{\hbar k_0\tau}{m}-\frac{\pi}{2k_0}\right)}\right.$$
$$\left.+\left[\frac{e^{i\Delta k\frac{1}{2}\left(\left(x_0-\frac{\hbar k_0T}{m}+\chi-\frac{\hbar k_0\tau}{m}+\frac{\pi}{2k_0}\right)\right)}-e^{-i\Delta k\frac{1}{2}\left(\left(x_0-\frac{\hbar k_0T}{m}+\chi-\frac{\hbar k_0\tau}{m}+\frac{\pi}{2k_0}\right)\right)}}{i\left(x_0-\frac{\hbar k_0T}{m}+\chi-\frac{\hbar k_0\tau}{m}+\frac{\pi}{2k_0}\right)}\right]e^{i\Delta k\frac{1}{2}\left(x_0-\frac{\hbar k_0T}{m}+\chi-\frac{\hbar k_0\tau}{m}+\frac{\pi}{2k_0}\right)}\right)e^{-i\frac{\hbar(T+\tau)}{2m}k_0^2}e^{ik_0x}.$$

(d3)

This is the final result that we described in chapter 4.

$$\psi(x,t)$$

$$= \begin{pmatrix} 4\sin c\left(\Delta k\frac{1}{2}\left(x_0-\frac{\hbar k_0 T}{m}+\chi-\frac{\hbar k_0\tau}{m}-\frac{\pi}{2k_0}\right)\right)e^{-i\frac{1}{2}\Delta k\left(x_0-\frac{\hbar k_0 T}{m}+\chi-\frac{\hbar k_0\tau}{m}-\frac{\pi}{2k_0}\right)} \\ +4\sin c\left(\Delta k\frac{1}{2}\left(x_0-\frac{\hbar k_0 T}{m}+\chi-\frac{\hbar k_0\tau}{m}+\frac{\pi}{2k_0}\right)\right)e^{-i\frac{1}{2}\Delta k\left(x_0-\frac{\hbar k_0 T}{m}+\chi-\frac{\hbar k_0\tau}{m}+\frac{\pi}{2k_0}\right)} \end{pmatrix} e^{-i\frac{\hbar(T+\tau)}{2m}k_0^2}e^{ik_0x}.$$

(d4)

Appendix E.

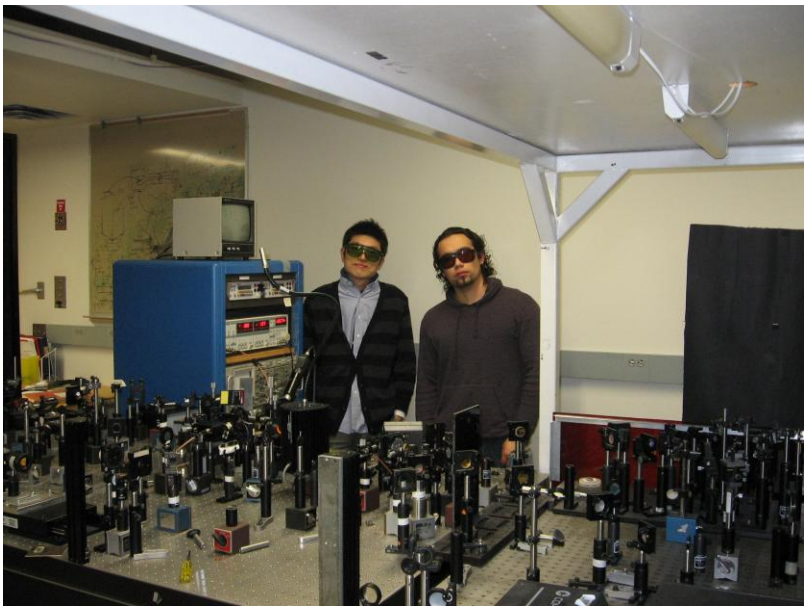

Fig. E1. Hiroshi Irie and the author, using the Optical instrumentation of our experimental setup, in UofR Laser Lab.

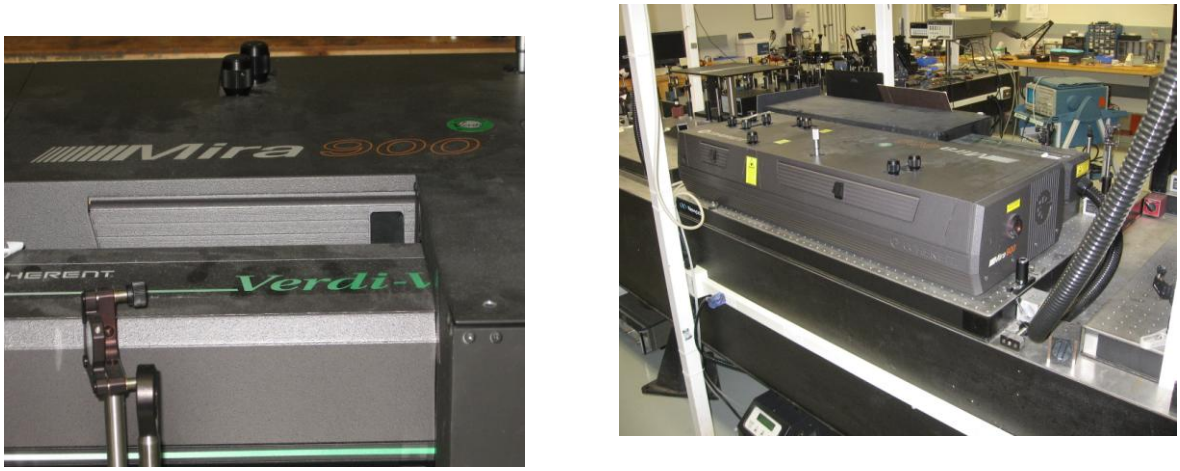

Fig. E2. The used lasers, Mira 900 and Verdi V10.

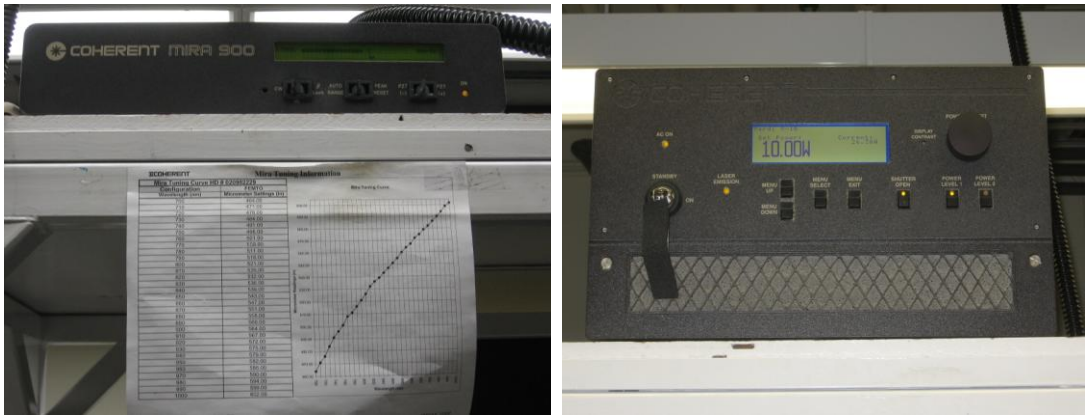

Fig. E3. Controller devices for the Coherent Mira 900(left) and Verdi V-10(right).

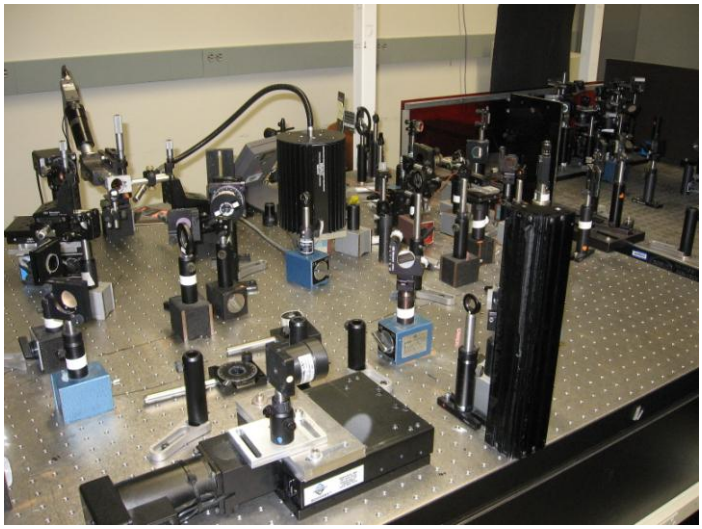

Fig. E4. Experimental setup with the delay station.

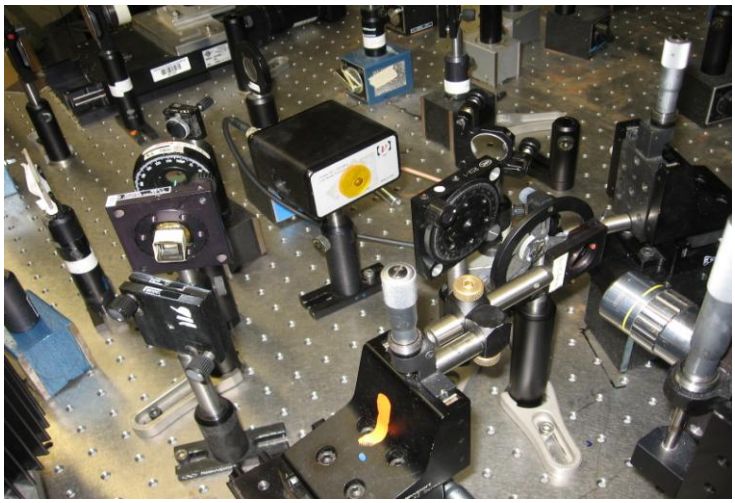

Fig. E5. Transmittance configuration and the sample on the 3D station.

References.

1. M. A. Stroscio and M. Dutta. *Phonons in Nanostructures*. 1st Ed., Cambridge University Press, 2001. Pp. 31
2. A. Yariv, *An Introduction to Theory and Applications of Quantum Mechanics*. 1st Ed. Wiley, New York, 1982. Pp. 237
3. J. P. Wolf. *Imaging phonons: acoustic wave propagation in solids.* 1st Ed., Cambridge University Press, Pp. 64
4. L. Saviot and D. B. Murray. *Long Lived Acoustic Vibrational Modes of an Embedded Nanoparticle*. Phys. Rev. Let. 93, 055506, 2004. Pp. 1-5
5. B. Jalali and S. Fathpour, *Silicon Photonics*, J.of lightwave tech., Vol. 24, No. 12, December 2006. Pp. 4600-4615
6. B. Jalalis. Yegnanarayanan, T. Yoon, T. Yoshimoto, I. Rendina, and F. Coppinger, *Advances in silicon-on-insulator optoelectronics*, IEEE J. of sel. Top. in quant. Elect., Vol. 4 No. 6, November/December 1998. Pp.938-947
7. G. K. Cellera, S. Cristoloveanu, *Frontiers of silicon-on-insulator,* Journal of applied physics volume 93, Number 9, 2003. Pp.4955-4978
8. W.P. Maszara, G Goetz, A Caviglia. *Bonding of silicon wafers for silicon-on-isulator.* J.of Appl.Phys. Vol 64, No10, 1998. Pp. 4943-4951
9. K. P. Gadkaree,a) K. Soni, S.C. Cheng, and C. Kosik Williams. *Single-crystal silicon films on glass*. J.of Mat. Res.Vol. 22, No. 9, 2007. Pp. 2363-2367
10. J.H. Cheon, S.H. Park, M. H. Kang, J. Jang, S. E. Ahn, Cites, C. Kosik Williams, and C. CheWang. *Ultrathin Si Thin-Film Transistor on Glass.* IEEE Elect. Dev. Let., Vol. 30, No. 2, 2009. Pp. 145-147

11. D. F. Dawson-Ellia, C. A. Kosik Williamsa, J. G. Couillarda, J. Citesa, R. G. Manleyb, G. Fengerb, and K. D. Hirschmanb. *Demonstration of High Performance TFTs on Silicon-on-Glass (SiOG) Substrate*. ECS Transactions, The Electrochemical Society, 8 (1) 223-228, 10.1149/1.2767312. 2007. Pp.1-6

12. O. Svelto. *Principles of Lasers.* Plenum Pressing Cooperation, 233 Spring, 4th edition, New York, NY, 1998. Pp. 661

13. S Garcia-Revilla, F Rodriguez, R Valiente and M Pollnau. *Optical spectroscopy of Al2O3:Ti3+ single cristal under hydrostatic pressure.* The influence on the Jahn–Teller coupling. J.l of Phys.: Condensed Matter 14, 2002. Pp. 447–459

14. L E Baush, I Vergara, F Jaque and J Garcia Sole. *Ultraviolet laser excited luminescence of Ti-sapphire*. J.l of Phys.: Condensed Matter 2, 1990. Pp. 9919-9925

15. Coherent, Inc. *MIRA900 Modelocked Ti: Sapphire Lasers.* http://www.coherent.com/downloads/Mira900_DS.pdf, USA, MC-135-02-2.5M0603, 2002. Pp.1-2

16. Coherent, Inc. *Manual Verdi TM V8/V10 Diode pumped lasers.* http://www.coherent.com/Downloads/Verdi_V8-V10_Preinstallation.pdf#page=13. Part No. 0175-452-00, Rev BB. USA 09/2005 Pp.1-11

17. T. Brabec, Ch. Spielmann, P. F. Curley, and F Krausz. Kerr *Lens mode locking.* Opt. Let./ Vol. 17, No. 18, 1992. Pp.1292-1294

18. W. Koechner. *Solid-state laser engineering,* Springer, New York, NY 6th edition, 1997. Pp. 538

19. J. Bird. *Higher engineering Mathematics*, Elsevier, Fifth edition, 2006. Pp 56

20. M. Csele. *Fundamentals of light sources and lasers and lasers*. Wiley, first edition, 2004. Pp. 215

21. R A Ganeev, A I Ryasnyansky, Sh R Kamalov, M K Kodirov and T Usmanov. *Nonlinear susceptibilities, absorption coefficients and refractive indices of colloidal metals*. J. Phys.D: Applied Physics. 2001. Pp. 1602-1611

22. T. Brabec, Ch. Spielmann, P. F. Curley, and F Krausz. Kerr *Lens mode locking*. Opt. Let. / Vol. 17, No. 18 / Sept. 15, 1992. Pp. 1292-1294

23. J. A. Valdmanis, R. L. Fork and J. P. Gordon. *Generation of optical pulses as short as 27 femtoseconds directly from a laser balancing self-phase modulation, group-velocity dispersion, saturable absorption, and saturable gain.* Opt. Let., Vol. 10, No. 3, March 1985. Pp. 131-133

24. G.P. Agrawal. *Fiber-optic communication systems*. Jhon wiley and sons, Inc. 3rd edition. Pp. 2

25. N. Delisie, D. Garlan. *A formal specification of an oscilloscope. Software,* Issue No. 5. 1990 Pp. 29-36

26. E. G. Loewen, E. P. McKnight. *Diffraction gratings and application*. Marcel Dekker Inc, 1997. Pp. 49

27. M. Lisowski, P.A. Loukakos, U. Bovensiepen, C. Gahl, M. Wolf. Ultra-*fast dynamics of electron thermalization, cooling and transport effects in Ru(001).* App.Phys. A 78, 2004. Pp. 165–176

28. M.Xie, Z. Yuan, B. Qian, and L. Pavesi. *Silicon nanocrystals to enable silicon photonics*, Chin. Opt. Let.: Vol. 7, No. 4, 2009. Pp 319-324

29. J.M. Martínez-Duart, R.J. Martín-Palma, F. Agulló-Rueda. *Nanotechnology for microelectronics and optoelectronics*, Elsevier 1st edition, San Diego, California. Pp.12

30. J.W. Precker, Marcilio A. da Silva. *Experimental estimation of the band gap in silicon and germanium from the temperature–voltage curve of diode thermometers Am*. J. Phys. 70-11, November, 2002. Pp. 1150-1153

31. G P Joshi, N S Saxena, R Mangal, A Mishra and T P Sharma. *Band gap determination of Ni–Zn ferrites*. Bull. Material Sciences, © Indian Academy Sciences, Vol. 26, No. 4, June 2003, pp. 387–389.

32. M. Sheike-Baha, D. J. Hagan, T. H. Wei, J. Wang, J. Young, and E. W. Van Stryland, *"Dispersion and band-gap scaling of electronic Kerr effect in solids associated with two-photon absorption,"* Phys. Rev. Let. 1990. Pp. 65- 96.

33. Tokmakoff, B. Sauter, and M. D. Fayer, *Temperature-dependent vibrational relaxation in polyatomic liquids: Picosecond infrared pump-probe experiments*. J. Chem. Phys. 100, 1994. Pp. 9035-9043

34. T. Sjodin, H. Petek, and H.L. Dai, *Ultrafast Carrier Dynamics in Silicon: A Two-Color Transient Reflection Grating Study on a (111) Surface*. Phys.Rev. Let. Volume 81, Number 25. Pp. 5664–5667

35. S. Karp, *Statistical properties of ensembles of classical wave packets*, J.Opt. Soc.of America, Volume 65, Number 4, 1975. Pp. 421-424

36. J. D. Jackson, *Classical Electrodynamics,* John Wiley & Sons, River Street, Hoboken, NJ. 1st edition. 1925. Pp.3

37. G. Kristensson, Ari Sihvola and Sten Rikte, *Mixing formulas in the time domain*, Vol. 15, No. 5. . J.Opt. Soc. America A. May 1998, Pp. 1411-1422

38. M. Fox, *Optical properties of Solids.* Oxford University Press, New York USA, 1st edition, 2001 Pp. 16.

39. D. E. Aspnes and A. A. Studna. *Dielectric properties of heavily doped crystalline and amorphous silicon from 1.5 to 6.0 eV*, Phys. Rev. B 27, 985, 198. Pp.768-779

40. P. Y. Yu, Manuel Cardona, *Fundamentals of semiconductor Physics and Materials Properties*, Springer, 3rd edition, Pp.206

41. C. Kittel, *Introduction to Solid State Physics*, John Wiley & Sons, Inc, Street, Hoboken, NJ. 8th Edition, 2005. Pp.136

42. B. E. A. Saleh, Malvin Carl Teich, *Fundamentals of Photonics*, John Wiley & Sons, Inc. Street, Hoboken, NJ, 1st edition,1991, Pp. 580

43. J.M. Martínez-Duart, R.J. Martín-Palma, F. Agulló-Rueda. *Nanotechnology for microelectronics and Optoelectronics*, Elsevier, San Diego, California, 1st edition. 2006. Pp.151

44. B. Jalali and S. Fathpour, *Silicon Photonics*, J. Lightwave tech. Vol. 24, No. 12, December 2006. Pp.4600-4615

45. J.H. Cheon, S. Hyun Park, M. Hyo Kang, J. Jang, S.E. Ahn, J. Cites, C. Kosik Williams, and C. CheWang. *Ultrathin Si Thin-Film Transistor on Glass*. IEEE Elec.Dev. Let. Vol. 30, No. 2, 2009. Pp.145-147

46. F. Marquardt, J. P. Chen, A. A. Clerk, and S. M. Girvin, *"Quantum Theory of Cavity-Assisted Sideband Cooling of Mechanical Motion",* Phys. Rev. let., vol 99, No093902, Pp. 1-4

47. B.A. Young, B. Cabrera, and A.T. Lee, *"Observation of ballistic phonos in silicon crystals induced by α particle"* Phys. Rev. let. vol 64, No 23, Pp. 2795-2798

48. C. Kittel,*"Introduction to solid state phys",* J. Wiley & Sons,1976.Pp. 19.

49. R. Biswas and V. Ambegaokar, *"Phonon Spectrum of a model of electronically excited silicon",* Phys. Rev. B, Vol.26, No 4, pp 26-35

50. L. I. Schiff, *"Quantum Mechanics",*McGraw Hill Book C.Inc.1949.Pp 12.

51. C.F Klingshirn, *"Semiconductor Optics",* Springer. 1992. Pp.102

52. C Thomsen, H.T. Grahan, H.J Marris, J. Tauc, *"Surface generation and detection of phonons by picoseconds light pulses",* Phys. Rev.B, Vol. 34, No 6, pp 4129-4137

53. T. R. Hart, L.R. Aggarwal, and B. Lax, *"Temperature dependence of Ramman Scattering in Silicon",* Phys. Rev. B, Vol. 1, No 2, Pp. 638-642

54. J. P. Wolfe, *"Imaging phonons, Acoustic wave propagation in solids"*, Cambridge University, 1998. Pp. 372

55. M. Lindgren, M. Currie, C. Williams, T. Y. Hsiang, P. M. Fauchet, R. Sobolewski, S. H. Moffat, R. A. Hughes, J. S. Preston, and F. A. Hegmann, *"Intrinsic picoseconds response times of Y-Ba-Cu-O" Superconducting detectors."* Appl. Phys. Let. Vol 74, No 6.Pp. 853-857.

56. S. Wu, P. Geiser, J. Jun, and J. Karpinski, J.-R. Park and Roman Sobolewski, *"Long-lived, coherent acoustic phonon oscillations in GaN single crystals"* Appl. Phys.Let. 88, 041917, 2006.

57. J. K. Miller, J. Qi, Y. Xu, Y.-J. Cho, X. Liu, J. K. Furdyna, I. Perakis, T. V. Shahbazyan, and N. Tolk, *"Near-bandgap wavelength dependence of long-lived traveling coherent longitudinal acoustic phonons in GaSb-GaAs heterostructures"*, Phys.Rev. B, Vol 74, 74, 113313, 2006

58. J. Herrin, J.S Howland, *"The Born–Oppenheimer Approximation: Straight-Up and with a Twist"*, Rev.Math.Phys. Volume: 9, Issue: 4. Pp. 467-488

59. E.M. Lifshitz and L.P Pitaevzki, *"Physical Kinetics"*, Pergamon press. Pp. 89

60. J.P. Wolfe, *"Imaging phonons, Acoustic wave propagation in solids"*, Cambridge University Press Pp. 25499